

The background of the entire page is a grayscale scanning electron microscope (SEM) image of numerous spherical micro-particles. The particles vary in size and some show surface irregularities or smaller particles attached to them, characteristic of ALD-coated particles. The lighting creates highlights and shadows, giving a three-dimensional appearance to the spheres.

Quantifying the Wettability of ALD-Coated Micro-Particles

Master Thesis Chemical Engineering
Pratyush Wanjari

Quantifying the Wettability of ALD-Coated Micro-Particles

by

Pratyush Wanjari

to obtain the degree of Master of Science,
at the Delft University of Technology,
to be defended on Friday, Jun 16th 2023 at 10:00 AM.

Student Number: 5337364

Project Duration: 1st Sept 2022 – 16th Jun 2023

Research Group: Product and Process Engineering

Thesis Committee: Prof. dr. ir. J. R. van Ommen

Dr. B. Bera

Dr. E. Hinderink

TU Delft, Full Professor, PPE

TU Delft, Assistant Professor, TP

TU Delft, Assistant Professor, P&E

Daily Supervisor: R. Kamphorst

TU Delft, PhD



ABSTRACT

This research aimed to enhance and quantify the wettability and water affinity of *Expancel* microparticles which generally demonstrates a lack of affinity with water. To enhance their water affinity, hydrophilic coatings like SiO₂ and TiO₂ were deposited onto the microparticles using atomic layer deposition (ALD). Various experimental techniques were employed to analyse the affinity, wettability, surface morphology, surface charge, and elemental compositions of the coated particles. TGA was conducted to examine the water affinity by subjecting the particles to direct heat in the temperature range of 25°C to 130°C under inert conditions. Weight loss% w.r.t temperature were measured, with a focus from the initial stage 25°C to 80°C, representing moisture loss from the surface. An increase in weight loss% was observed for SiO₂ samples as the number of coating layers increased, indicating enhanced affinity with water. SEM images were captured at different temperatures of 80°C, 100°C, and 130°C to clarify and explain the trend observed in TGA graphs. It was discovered that there is no expansion until 80°C, full expansion at 100°C, and particle ruptures at 130°C due to the fact that the encapsulated gas escapes the particles completely. Experiments to measure WCA were conducted to quantify the wettability of coated particles and compare them to uncoated particles. The data indicated improved wettability for SiO₂ and TiO₂-coated particles, as evidenced by reduced contact angles. As *Expancel* microparticles tend to agglomerate in the presence of water, focused beam reflectance measurement (FBRM) analysis was employed to measure real-time agglomerate size. The FBRM measurements demonstrated reduced agglomerate sizes for coated particles compared to uncoated particles. XPS analysis was used to examine the elemental compositions on the particle surface after coating with varying no. of coating layers; higher silicon (Si) concentrations were found as compared to titanium (Ti). ICP-EOS was used to quantify the amount of Si and Ti weight% after varying no. of deposition layer. The data indicated that the amount of Si was measured to be a lot more than the theoretical value, which implied CVD behaviour in our reactor. LEIS analysis revealed that one layer of coating achieved full surface coverage with SiO₂, and subsequent coating cycles did not significantly alter the surface composition.

CONTENTS

1 INTRODUCTION	1
1.1 Scope of The Research	1
1.2 Thesis Report Outline	1
2 THEORETICAL BACKGROUND	2
2.1 Expancel	2
2.2 Atomic Layer Deposition	3
2.2.1 General	3
2.2.2 Reaction.....	4
2.3 Characterisation Techniques	5
2.3.1 Water Contact Angle.....	5
2.3.2 Thermogravimetric Analysis (TGA).....	6
2.3.3 Scanning Electron Microscopy (SEM)	7
2.3.4 Zeta Potential Measurement	8
2.3.5 Focused-Beam Reflectance Measurement (FBRM).....	9
2.3.6 Inductively Coupled Plasma Spectroscopy (ICP)	10
2.3.7 X-Ray Photoelectron Spectroscopy (XPS).....	10
2.3.8 Low-Energy Ion Scattering (LEIS)	10
3 METHODOLOGY	11
3.1. Atomic Layer Deposition	11
3.1.1 Experimental Setup	11
3.1.2 Conditions and Parameters	12
3.1.3 Collecting The Sample	12
3.2 Thermogravimetric Analysis	13
3.3 Scanning Electron Microscopy	13
3.4 Water Contact Angle	13
3.5 Zeta Potential	14
3.6 Focused Beam Reflectance Measurement	14
4 RESULTS AND DISCUSSION	15
4.1 Thermogravimetric Analysis	15
4.2 Scanning Electron Microscopy	17
4.3 Zeta Potential	19
4.4 Contact Angle Measurements	19
4.5 Focused Beam Reflectance Measurements	20
4.6 X-Ray Photoelectron Spectroscopy	29
4.7 Low Energy Ion Scattering	30
4.8 Inductively Coupled Plasma	23
5 CONCLUSION AND RECOMMENDATION	25
REFERENCES	27

APPENDICES30

A USER MANUAL.....31

A Experimental Procedure.....31

 A.1.1 Atomic Layer Deposition.....31

 A.1.2 Thermogravimetric Analysis..... 31

 A.1.3 Water Contact Angle.....32

 A.1.4 Scanning Electron Microscopy..... 32

 A.1.5 Focused Beam Reflectance Measurement.....33

 A.1.6 Zeta Potential..... 33

B EXPERIMENTAL SETUP34

C CONTACT ANGLE MEASUREMENTS.....38

D ZETA POTENTIAL DISTRIBUTION.....39

E WETTING TIME.....43

LIST OF FIGURES

Figure 2.1 Expancel microspheres from 12 μm to 40 μm when exposed to heat.....	2
Figure 2.2 SEM images of Expancel at room temperature (showing no expansion) and at elevated temperature (showing expansion).....	3
Figure 2.3 Chemical structure of the two monomers that form Expancel polymer	3
Figure 2.4 One complete cycle of ALD.....	4
Figure 2.5 Schematic overview of a fluidized bed reactor used for ALD.	5
Figure 2.6 Sessile drop on the pellet for measuring WCA.	6
Figure 2.7 General representation of TGA plot of Weight Loss% Vs Temperature of uncoated Expancel.....	7
Figure 2.8 SEM - BEC Image and EDS Elemental Mapping of TiO_2 - coated Expancel	7
Figure 2.9 Schematic representation of zeta potential.....	8
Figure 2.10 Schematic zeta potential Vs pH plot indicating isoelectric point.....	9
Figure 2.11 Schematic sketch of FBRM probe.	9
Figure 3.1 Flowsheet of ALD experiment	19
Figure 3.2 SEM Images depicting agglomeration of SiO_2 and TiO_2 coating.....	20
Figure 4.1.1 TGA Plot for Expancel Uncoated from 25°C – 130°C and SEM images at temperatures 80°C, 100°C, 130°C. 15	
Figure 4.1.2 TGA Plot for Expancel from 25°C – 130°C and SEM images 1, 2, 3 at temperatures 80°C, 100°C, 130°C; a) with SiO_2 coating, b) with TiO_2 coating.....	16
Figure 4.2 SEM Images of Expancel at 2500x with varying temperatures.....	19
Figure 4.4 Contact angle measurements of uncoated, SiO_2 and TiO_2 coated particles Vs no. of cycles.....	19
Figure 4.5 FBRM measurement plots indicating the agglomerate size (μm)Vs varying no of cycles.....	21
Figure 4.6 XPS plot indicating the atomic concentration percentage of different elements Vs varying no. of cycles.....	22
Figure 4.7 LEIS spectra for uncoated and SiO_2 1C, 2C and 100C coated microparticle and SEM Image of SiO_2 1C sample.23	
Figure 4.8 Plot for ICP denoting weight% of titanium and silicon w.r.t varying no. of cycles.....	24
Figure B. 1 ALD experimental setup in the lab.....	34
Figure B. 2 Fluidised bed reactor mounted on a vibrating table.....	35
Figure B. 3 Expanded Expancel due to exothermic reaction.....	35
Figure B. 4 Thermal Analysis System TGA - 2 by Mettler Toledo GmbH.....	36
Figure B. 5 Scanning Electron Microscope - Joel JSM - 6010LA.....	36
Figure B. 6 Powder Pelletising Die.....	37
Figure B. 7 Experimental setup for measuring WCA.....	37
Figure B. 8 Powder Mixed in 200mL MilliQ Water.....	37
Figure B. 9 Experimental setup of FBRM.....	37
Figure D.1 Zeta Potential (mV) Vs total counts(kcps) for uncoated sample.....	39
Figure D.2 Zeta Potential (mV) Vs total counts(kcps) for SiO_2 1C sample.....	39
Figure D.3 Zeta Potential (mV) Vs total counts(kcps) for SiO_2 2C sample.....	39
Figure D.4 Zeta Potential (mV) Vs total counts(kcps) for SiO_2 3C sample.....	39
Figure D.5 Zeta Potential (mV) Vs total counts(kcps) for SiO_2 4C sample.....	40
Figure D.6 Zeta Potential (mV) Vs total counts(kcps) for SiO_2 5C sample.....	40
Figure D.7 Zeta Potential (mV) Vs total counts(kcps) for SiO_2 10C sample.....	40
Figure D.8 Zeta Potential (mV) Vs total counts(kcps) for TiO_2 1C sample	40
Figure D.9 Zeta Potential (mV) Vs total counts(kcps) for TiO_2 2C sample.....	41
Figure D.10 Zeta Potential (mV) Vs total counts(kcps) for TiO_2 3C sample.....	41
Figure D.11 Zeta Potential (mV) Vs total counts(kcps) for TiO_2 4C sample.....	41
Figure D.12 Zeta Potential (mV) Vs total counts(kcps) for TiO_2 5C sample.....	41

Figure D.13 Zeta Potential (mV) Vs total counts(kcps) for TiO ₂ 10C sample.....	42
Figure E. 1 Wetting Time (sec) Vs No. of Attempts of Uncoated Samples.....	43
Figure E. 2 Wetting Time (sec) Vs No. of Attempts of SiO ₂ 1C Samples.....	43
Figure E. 3 Wetting Time (sec) Vs No. of Attempts of SiO ₂ 2C Samples.....	43
Figure E. 4 Wetting Time (sec) Vs No. of Attempts of SiO ₂ 3C Samples.....	43
Figure E. 5 Wetting Time (sec) Vs No. of Attempts of SiO ₂ 4C Samples.....	44
Figure E. 6 Wetting Time (sec) Vs No. of Attempts of SiO ₂ 5C Samples.....	44
Figure E. 7 Wetting Time (sec) Vs No. of Attempts of SiO ₂ 10C Samples.....	44
Figure E. 8 Wetting Time (sec) Vs No. of Attempts of TiO ₂ 1C Samples.....	44
Figure E. 9 Wetting Time (sec) Vs No. of Attempts of TiO ₂ 2C Samples.....	45
Figure E. 10 Wetting Time (sec) Vs No. of Attempts of TiO ₂ 3C Samples.....	45
Figure E. 11 Wetting Time (sec) Vs No. of Attempts of TiO ₂ 4C Samples.....	45
Figure E. 12 Wetting Time (sec) Vs No. of Attempts of TiO ₂ 5C Samples.....	45
Figure E. 13 Average Wetting Time (sec) Vs Different Samples.....	46

LIST OF TABLES

Table 4.1 Measured TGA data of uncoated, SiO ₂ and TiO ₂ -coated Expancel from the initial temperature to onset -1, onset -1 to onset 2, and overall weight loss%.....	17
Table C.1 Measured water contact angle (WCA) of uncoated, SiO ₂ and TiO ₂ -coated Expancel.....	38

1

INTRODUCTION

Expancel is a commercial product manufactured by Nouryon. This micro-powder has a low-density core polymer that encapsulates the gas, surrounded by a thin, robust shell that gives particles excellent resistance to compression and collapse. When particles are exposed to heat, they tend to expand up to 60 times their original size [1]. This is because the shell that encapsulates the gas softens, and the pressure of the gas inside the hollow sphere increases, resulting in the dramatic expansion of the powder. This expanded powder has the same weight while covering a larger volume. This exceptional property makes it suitable for applications such as a lightweight filler, blowing agent or inks and pigments for paintings. However, *Expancel* exhibits limited affinity with water, which results in reduced wetting and dispersion effects. When exposed to water, the polymer powder has a tendency to agglomerate or segregate, thereby hindering efficient dispersion and limiting the applicability of the powder in water. This poses a problem when using it, for example, in waterborne paint.

To overcome this limitation and broaden its potential applications, it is necessary to modify the surface properties of *Expancel* while preserving its specific bulk properties. One viable approach to enhance its affinity with water is to apply an ultra-thin coating of an inorganic substance with highly hydrophilic characteristics using Atomic Layer Deposition (ALD). It is a technique for depositing ultra-thin coatings in the nanometre range by employing sequential exposures of precursors to the surface. ALD achieves precise control over the thickness of the coating based on the performance of the system and the number of cycles conducted. This method is well suited, as it ensures that the weight of the powder remains largely unaffected, thus preserving its inherent bulk qualities.

Thus, this study was undertaken with the objectives:

- To quantify the wettability of *Expancel*
- To analyse the surface of coated particles using various characterisation techniques such as SEM, XPS, LEIS, ICP-EOS
- To evaluate the affinity with water and wetting behaviour of the coated particles using TGA, WCA and FBRM techniques
- To determine which coating gives optimal results (increase in affinity and decrease in agglomeration) concerning wettability.

1.1 Scope of The Research

The focus of this project is specifically on the predetermined coating method, ALD, and therefore, exploring alternative coating techniques to enhance particle wettability falls beyond the scope of this study. However, considering the objectives of the study, the characterization techniques to be employed include Thermogravimetric Analysis (TGA) for assessing water affinity, Scanning Electron Microscopy (SEM) for studying surface morphology, Water Contact Angle (WCA) measurements to evaluate wettability and surface energy of *Expancel*, Zeta Potential for determining surface charge, and Focused Beam Reflectance Measurement (FBRM) for monitoring agglomeration and phase segregation over time.

1.2 Thesis Report Outline

The report commences with the [Theoretical Background](#), providing the essential knowledge required to understand the conducted experiments and the subsequent results. This is followed up by the [Methodology](#) section, outlining the procedures involved. The observations and their interpretation are then discussed in the [Results & Discussion](#) section. Finally, the report concludes with concluding remarks in the [Conclusions section](#).

2

THEORETICAL BACKGROUND

This chapter includes the necessary background information for comprehending the study and the conducted experiments. The section begins with an overview of the *Expancel* product, followed by an explanation of the fundamental principles of ALD, wettability, and various characterization techniques such as TGA, SEM, Zeta Potential, and FBRM. These topics are further explored and discussed in detail within this chapter.

2.1 Expancel

Expancel is a commercial product manufactured by Nouryon. It is a thermoplastic hollow microsphere encasing a gas within its centre. When subjected to heat, the gas inside the microsphere expands, causing a significant increase in the volume, as illustrated in Figure 2.1. The polymer shell exhibits elasticity when it reaches the glass transition temperature, which is approximately 80°C. Upon cooling, the shell hardens, and the microsphere retains its enlarged shape. This unique property allows *Expancel* to expand up to 60 times its original volume without a significant increase in weight. [1].

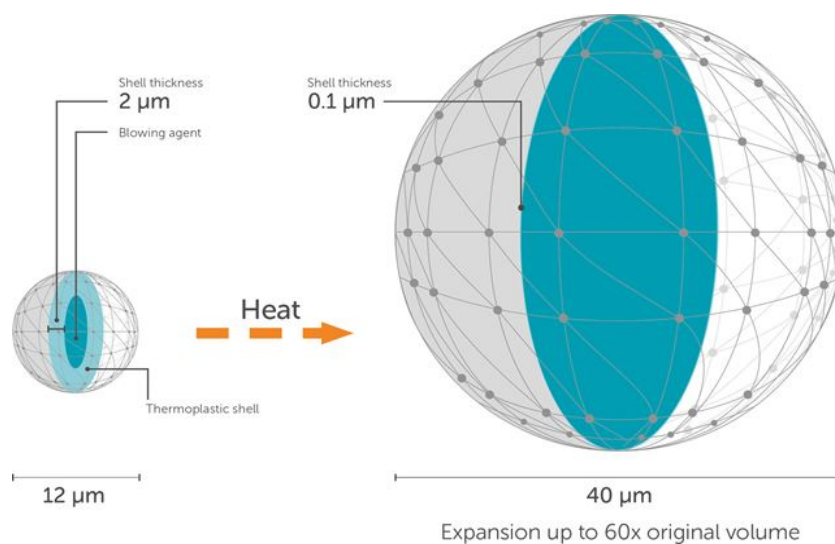


Figure 2.1 *Expancel*/microsphere from 12 μm to 40 μm when exposed to the heat [1]

The SEM images in Figure 2.2 illustrate the initial state of *Expancel* at room temperature, i.e. 25°C, where no expansion is observed, retaining its original shape and structure. However, when it is exposed to elevated temperature, i.e. 100°C, we can observe an increase in the volume of the microsphere, highlighting the expansion phenomenon in response to the heat.

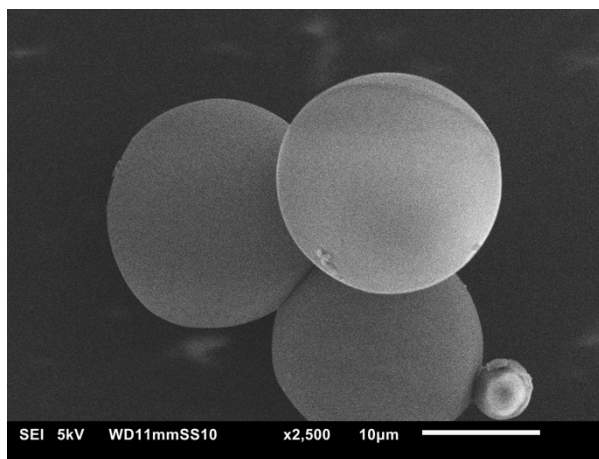
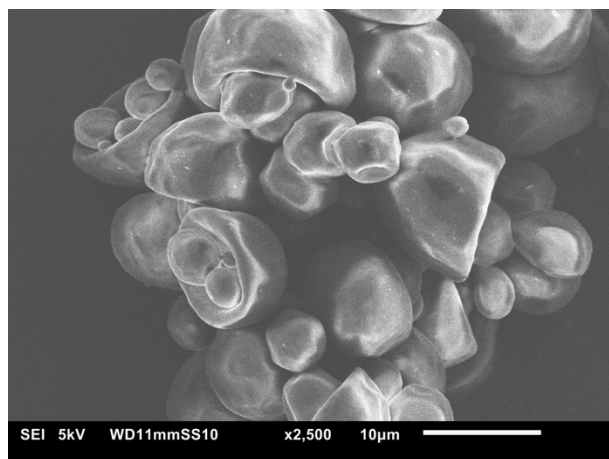


Figure 2.2 (a) SEM image of *Expancel* at room temperature (25°C)

Figure 2.2 (b) SEM image of *Expancel* at elevated temperature (100°C)

Figure 2.2 SEM images of *Expancel* at room temperature (showing no expansion) and at elevated temperature (showing expansion)

The particles are approximately 10-15 μm at room temperature. The shell of the polymer has a thickness of 2 μm and decreases in thickness when the microsphere is expanded. When it reaches its maximum expansion (i.e. 60 times the original size), the shell thickness is reduced to 0.1 μm . The shell of the polymer is generated by radical polymerization of the monomers acrylonitrile and methyl methacrylate (refer to figure 2.3). The polymer substrate has no affinity for water and serves as a protective and impermeable shell, allowing the gas to remain within and keep the particles floating. The density of the regular particles is 1100 kg/m^3 , and the density of the expanded particles is 30 kg/m^3 .

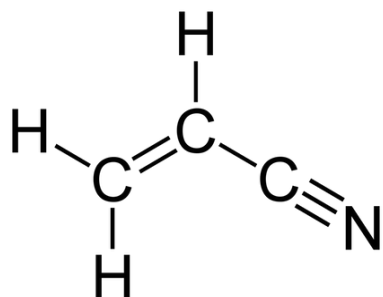


Figure 2.3 (a) Acrylonitrile

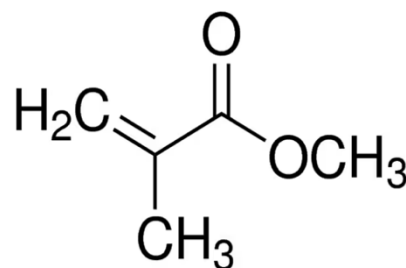


Figure 2.3 (b) Methyl methacrylate

Figure 2.3 Chemical structure of the two monomers that form *Expancel* polymer. (a) Acrylonitrile & (b) Methyl methacrylate

2.2 Atomic Layer Deposition

This section gives background information on the most important aspects of Atomic Layer Deposition (ALD).

2.2.1 General

Atomic Layer Deposition (ALD) is a method that dates back to the 1960s and 1970s. Two research groups, one in the Soviet Union and the other in Finland, independently discovered the layering technique [2]. Initially referred to as Atomic Layer Epitaxy (ALE), which translates to "on arrangement" and implies the deposition of one crystalline film over a crystalline substrate[3, 4]. However, it was discovered that most of the reactions resulted in amorphous films rather than epitaxial growth. As the technique evolved, it became known as Atomic Layer Deposition (ALD), becoming the dominant method for layer deposition.

ALD is employed to deposit uniform and conformal thin layers of materials onto a substrate. It shares similarities with Chemical Vapor Deposition (CVD) in that both techniques involve sequential, self-limiting surface reactions between a substrate and precursor. The reaction tends to continue until a monolayer of material is deposited. One notable advantage of ALD is its ability to modify the surface properties of a material while preserving its bulk properties. This feature expands the range of applications for various materials, enabling the adjustment of surface properties such as

conductivity, chemical reactivity, and wettability. ALD consists of four steps, where the precursor pulses are alternated with purge steps. In contrast, a different method called Chemical Vapor Deposition (CVD) involves simultaneous exposure of both precursors. This method is based on binary reactions [3]. ALD typically results in a thin layer between 0.1nm and 100nm, depending on the number of cycles, CVD applies a thicker layer ranging between 100nm and 100µm [6]. Furthermore, ALD coatings exhibit excellent uniformity due to the self-limiting reaction and the step-wise precursor pulse, resulting in the deposition of only one layer per cycle. Whereas, using CVD, the layers are formed as a function of reaction time because the precursors are exposed to the surface simultaneously. Also, the layer growth occurs locally, which results in a non-uniform layer and a larger coating thickness.

While ALD can be applied to a variety of surfaces, including nano-powders, flat substrates, and even nanotubes, this study focuses on the polymer microsphere surface of *Expancel*. Due to the organic content on the polymer surface, it exhibits low affinity with water. And introducing an ALD layer will seek to enhance its hydrophilicity. Previous studies have demonstrated that coating microspheres with inorganic materials such as silica (SiO₂) or titania (TiO₂) improve particle wettability [5]. Hence, the chosen precursors will enhance the hydrophilicity of *Expancel*.

2.2.2 Reaction

Atomic Layer Deposition is a technique where a thin layer on a nanoscale is deposited over a substrate by exposing a surface to gaseous reactants. This technique is based on self-limiting surface reactions, which form a coating by performing a sequential reaction cycle. This process can then be repeated multiple times to build up the desired thickness of the film. One cycle of an ALD reaction generally consists of four steps: (1) pulse of the first precursor; (2) purge; (3) pulse of the second precursor; (4) purge. One entire cycle can be seen in Figure 2.4 [5]. One complete reaction cycle is divided into two half-reactions. In this case of TiCl₄, equation 2.1 represents the first precursor pulse in which chlorides replace hydroxyls, and Ti-O bonds are formed, and equation 2.2 illustrates the second precursor pulse of H₂O; these H₂O molecules react with chlorides and generate new hydroxyls.

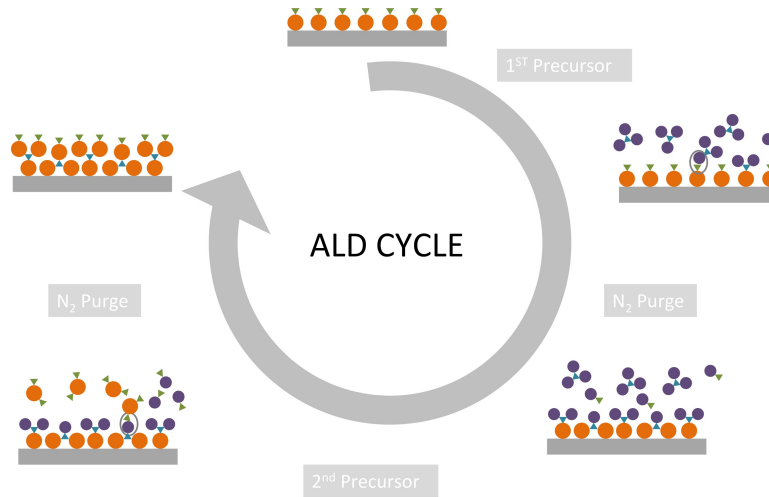
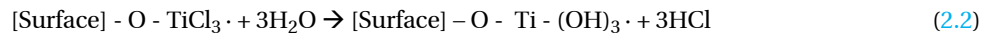


Figure 2.4 One complete cycle of ALD. (1) top right is the first precursor (SiCl₄ or TiCl₄) pulse, (2) N₂ a purge step, (3) bottom is the second precursor (H₂O) pulse and (4) N₂ purge step.

This study aims to assess the wettability of SiO₂ and TiO₂-coated *Expancel* utilizing silica tetrachloride (SiCl₄) and titanium tetrachloride (TiCl₄) as primary precursors. Another precursor employed in this process is H₂O, which acts as an oxidant, and N₂, a carrier gas used for purging, ensuring the removal of surplus precursors. For successful layer deposition, the substrate surface requires nucleation sites for the precursor to react. Hence, the initial cycles of ALD involve reactions between surface groups (-OH) and the precursors. As the process continues, layers are built upon previously deposited layers, resulting in continuous growth known as Growth Per Cycle (GPC) [7]. The applied coating thickness using ALD is usually between angstroms and nanometres [4, 8]. ALD creates strong covalent bonding between

the layers, ensuring in good adhesion [10]. This adsorption is called chemisorption, where a chemical bond is formed between the precursor and the substrate. Another type of adsorption that can occur is physisorption, which is driven by intermolecular forces such as van der Waals attractions [11]. When utilizing CVD, physisorption between the precursor and substrate occurs more frequently since the precursors are introduced simultaneously. However, due to the covalent forces involved in chemisorption, ALD will offer a stronger coating compared to CVD.

ALD reactions are typically performed at high temperatures to maximise the reaction's rate. However, in cases where the substrate properties do not allow for high-temperature operation, low-temperature ALD (LT-ALD) is employed, which involves temperatures below 100°C [13]. Considering the properties of *Expancel*, a temperature-sensitive polymer that begins expanding at 80°C, and the exothermic nature of the reaction between the precursor and substrate, it was decided to perform the ALD experiments at 50°C. One significant disadvantage of this approach is the lengthy purge times to prevent CVD. The longer purge times are a result of the slow desorption rates at low temperatures [4,14]. However, even with larger purge times, there is always a risk of CVD occurring on the particle surface within the reaction chamber, as physisorbed reactants are not easily purged.

Depending on the substrate and required productivity, a variety of reactor types are available. The purpose of the reactor chamber is to provide the necessary environment for allowing the reactant gases to efficiently reach and react with the substrates under process conditions that ensure ALD (12). In our specific case, when dealing with micro-powders, a fluidized bed reactor is preferred. Utilizing a fluidized bed for ALD offers several advantages, including efficient heat transfer, increased surface area (to achieve a more uniform deposition), and improved reaction kinetics, which contribute to achieving the desired product. In the reactor, the precursors enter the column from the bottom, causing them to fluidize and mix with the gas. This arrangement ensures uniform exposure of the solid particles to the precursor gas, resulting in uniform film deposition. A schematic image of a fluidized bed used for ALD is seen in figure 2.5.

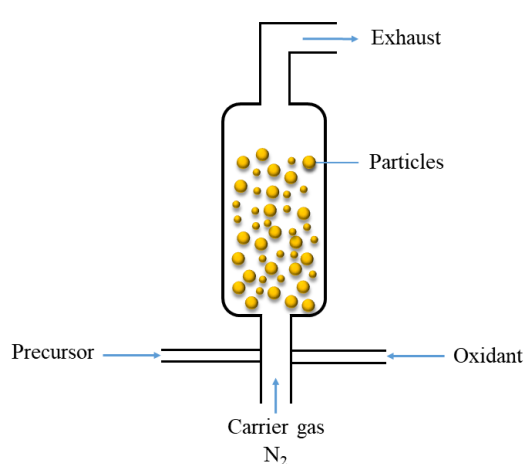


Figure 2.5 Schematic overview of a fluidized bed reactor used for ALD.

2.3 Characterisation Techniques

This section explains the key characterisation techniques used throughout this study, which will be beneficial for evaluating the obtained results.

2.3.1 Water Contact Angle

Wettability helps quantify the capacity of liquids to interact with solid surfaces. It determines the amount of wetting between solid and liquid phases that can be determined by measuring the water contact angle, which is used to evaluate the hydrophilicity or hydrophobicity of a material's surface. A lower contact angle ($<90^\circ$) indicates greater wettability or hydrophilicity, while higher contact angles ($>90^\circ$) indicate lower wettability or hydrophobicity. A low water contact angle on a surface indicates high hydrophilicity, implying that the water droplet spreads over a large area on the surface instead of forming a spherical bead as it would on a hydrophobic surface. The contact angle is defined as the angle formed between the liquid-air interface and the solid-liquid interface at the three-phase contact line. A low contact angle signifies that the solid-liquid interface is nearly flat, indicating significant wetting of the liquid on the surface.

Wettability can be calculated using many techniques, including the conventional telescope-goniometer and drop-shape analysis methods [16]. When a droplet makes contact with a surface, as shown in Figure 2.6, the energies of the

three-phase contact line are reduced to a minimum, causing the tangent of the droplet surface to create a distinct angle of contact with the outer surface, as described by Young's equation:

$$\gamma^{SV} - \gamma^{SL} = \gamma^{LV} \cos(\theta) \quad (2.3)$$

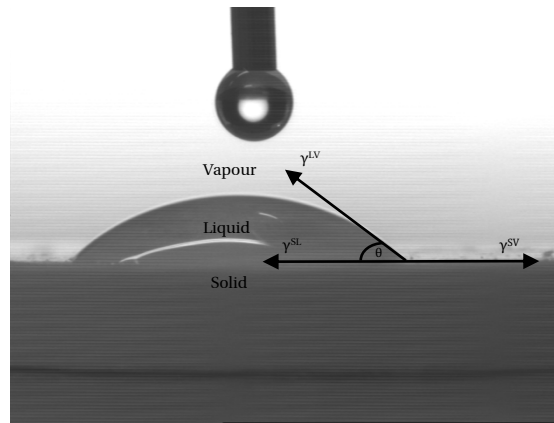


Figure 2.6 Sessile drop on the pellet for measuring WCA where γ^{LV} is the liquid surface free energy; γ^{SV} is the solid surface free energy; γ^{SL} is the solid/liquid interfacial free energy; θ is the contact angle

We may infer from equation 2.3 that a fluid will wet a surface if its surface energy is less than the difference between the solid-vapour and solid-liquid interfacial energies (this value is known as the critical surface tension). Any non-uniformity (physical or chemical) can cause the actual value to differ.

WCA and wetting time are significant parameters in describing surface wettability. WCA measures the angle between the liquid-air interface and the solid surface, indicating the hydrophobic or hydrophilic nature of the surface. Wetting time, on the other hand, refers to the duration for a liquid droplet to spread, in our case, it is sinking into the pellet making it completely wet. WCA and wetting time are interconnected, as the WCA value influences the wetting time. A hydrophobic surface with a high WCA value will have a longer wetting time compared to a hydrophilic surface with a low WCA value.

To determine wettability, the water contact angle (WCA) is measured to establish how SiO_2 and TiO_2 coating influences these contact angles. To measure the contact angle, the powder is pelletized, which involves compacting the powder into a flat and uniform surface. This method ensures accurate contact angle measurements of a stationary liquid droplet on the surface and minimizes the impact of surface roughness on contact angle measurement. Typically, the conventional analytical method of the sessile drop can be employed to measure the WCA. A small droplet of liquid is placed on the pellet's surface for the sessile drop test, as depicted in Figure 2.6. The contact angle between the liquid and the solid surface is then measured. This measurement indicates the wetting behaviour of the liquid on the solid surface and provides insights into the surface's wettability. Considering the objective of enhancing the hydrophilicity of the coated particles, we expect low contact angles with water. However, WCA on powders is not considered a reliable indicator of water affinity due to the parameters such as porosity and surface roughness. Thus, we do not use this method as the only indication of wettability.

2.3.2 Thermogravimetric Analysis (TGA)

Thermogravimetric analysis (TGA) is a technique employed to measure the mass of a substance in relation to temperature or time. This is done by subjecting the sample specimen to a controlled temperature program in a controlled environment. TGA consists of a sample pan that is supported by a precision balance. During the experiment, the pan undergoes heating or cooling in a furnace, and the mass of the sample is continuously measured. The sample environment is regulated by a purge gas, which flows over the sample and escapes through an exhaust. This gas can be inert or reactive in nature.

This analytical approach enables the quantification of various factors such as loss of water, loss of solvent, loss of plasticizer, decarboxylation, pyrolysis, oxidation, decomposition, weight % filler, amount of metallic catalytic residue left on carbon nanotubes, and weight % ash [19]. From the working principle of TGA, we can effectively evaluate the weight loss percentage of both uncoated and coated *Expancel*, as well as determine the amount of water present in the

sample and how it varies with increasing temperature. As the temperature rises, the volatile components evaporate, leading to a decrease in the sample's weight. This weight change provides insights into the amount of water present in the sample and its interaction with the substrate. Moreover, different outcomes can be observed at increasing temperatures depending on the properties of the substrate. Furthermore, figure 2.7 presents a general representation of the TGA plot of weight loss% vs temperature. Further details explaining this plot will be discussed in section 4.1.

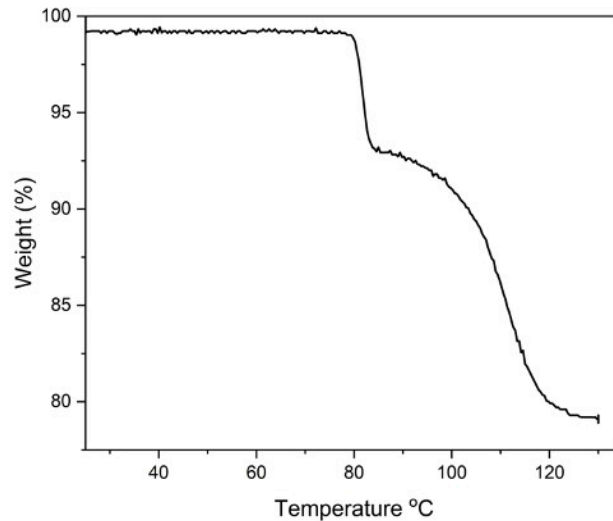


Figure 2.7 General representation of TGA plot of Weight Loss% Vs Temperature of uncoated Expancel.

2.3.3 Scanning Electron Microscopy (SEM)

Scanning Electron Microscopy (SEM) is a technique that utilizes a focused electron beam to scan the surface of a sample, generating highly detailed and magnified two-dimensional images. The electron beam is directed towards a specific area of the solid sample's surface, leading to interactions between the electrons and the sample. These interactions produce various signals that are captured by a detector, allowing for digital representations of the sample's morphology and topology. [20]. SEMs can potentially magnify specimens up to 300,000 times [21]. However, it should be noted, however, that the coating thickness cannot be directly determined using SEM since it only analyses the surface.

In addition to surface imaging, SEM can be combined with other analytical methods, such as Energy Dispersive X-Ray Spectroscopy (EDS), shown in Figure 2.8(b), to provide sample compositional information. In this context, the intensity of the green colour indicates the concentration or quantity of TiO_2 coating present on the particle. A brighter or more intense green colour corresponds to a higher amount of TiO_2 coating on the particle's surface. This enables a more thorough examination of surface morphology, including the distribution of various components on the surface.

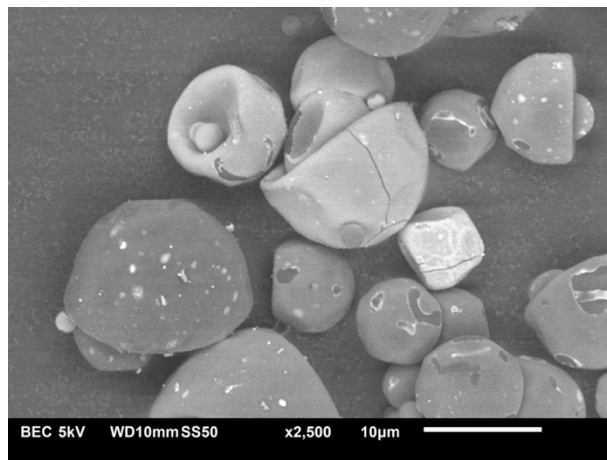


Figure 2.8 (a) SEM-BEC image of TiO_2 -coated Expancel



Figure 2.8 (b) EDS Elemental Mapping of TiO_2 -coated Expancel

Figure 2.8 SEM - BEC Image and EDS Elemental Mapping of TiO_2 - coated Expancel

2.3.4 Zeta Potential Measurement

The zeta potential also referred to as the electrokinetic potential, is a measure of the electrical potential difference between the surface of a charged particle in suspension. It reflects the degree of electrostatic repulsion between particles. It can be used to optimize the formulations of suspensions and emulsions, predict surface interactions, and optimise the formation of films and coatings. The measurements are performed while an electric field is applied to a dispersion of the material in an appropriate dispersion medium [23].

Within the liquid layer surrounding the particle, there are two distinct regions: an inner area known as the stern layer, where the ions are closely bonded, and an outer region referred to as the diffuse layer, where the ion is less closely bonded. The ions and particles form a stable entity within the diffuse layer due to a notional barrier. Ions inside the border move when a particle moves (for example, due to gravity). The ions that cross the border remain in the bulk dispersant. The zeta potential is potential at this border (surface of hydrodynamic shear) shown in Figure 2.9 [24].

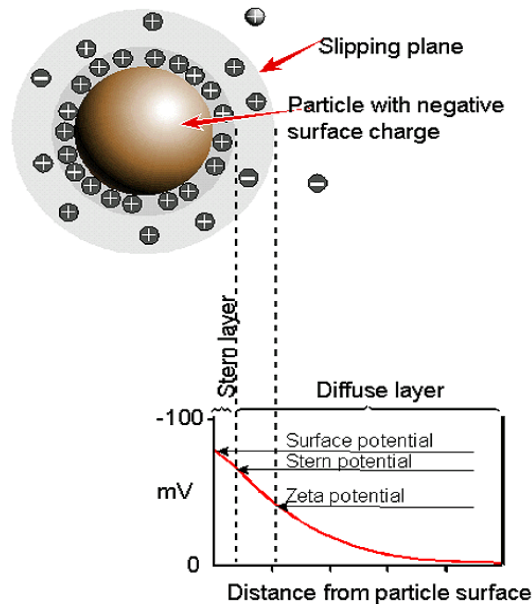


Figure 2.9 Schematic representation of zeta potential [24]

There is a broad dividing line between stable and unstable suspensions that is generally set at +30 or -30 mV. When the zeta potential has a high absolute value (either positive or negative), it indicates strong repulsive forces between particles and is often considered stable. This electrostatic repulsion counteracts the attractive van der Waals force by preventing the particles from coming close together, thereby reducing the likelihood of particle aggregation.

The zeta potential is influenced by the type of dispersion as well as the characteristics of the surface. Previous studies suggest that polymer surfaces generally exhibit lower surface charge density and indicate reduced hydrophilic behaviour. For example, surfaces composed of SiO_2 are hydrophilic and tend to have a high charge density. The literature also demonstrates that using ALD with metal oxides, such as SiO_2 and TiO_2 , can enhance the hydrophilicity of surfaces [25 - 32]. Consequently, when comparing the zeta potential of different materials, it is crucial to consider not only the particle's zeta potential but also provide details about the dispersant and the dispersion medium's properties. There are certain factors which might influence zeta potential, one such factor is pH.

The pH of a sample has a significant impact on its zeta potential when it is suspended in an aqueous medium. In the case of a particle suspended in water with a negative zeta potential, the addition of alkali to the suspension results in an increase in the negative charge of the particles. If acid is added to this suspension, it will reach to a point where the charge will be neutralized. Conversely, the introduction of acid to the suspension will eventually neutralize the charge. However, if more acid is added, it may lead to a build-up of positive charge if specific ions are adsorbed onto the particles' surfaces. As a result, a zeta potential versus pH curve will exhibit a positive value at low pH and a negative value at high pH. The point where the plot intersects the zero zeta potential is known as the isoelectric point, which holds practical significance. It is often the critical point where particle aggregation becomes highly probable, making the colloidal system less stable.

In Figure 2.10, a representative graph illustrating the relationship between zeta potential vs pH. The isoelectric point of the material, in this case, is about pH 5.5. Furthermore, the figure may be used to anticipate whether the sample will

be stable at pH values less than 4 (sufficient positive charge) or greater than pH 7.5. (sufficient negative amount is present). Dispersion stability issues would be predicted at pH values ranging from 4 to 7.5, with zeta potentials ranging from +30 to -30mV [24].

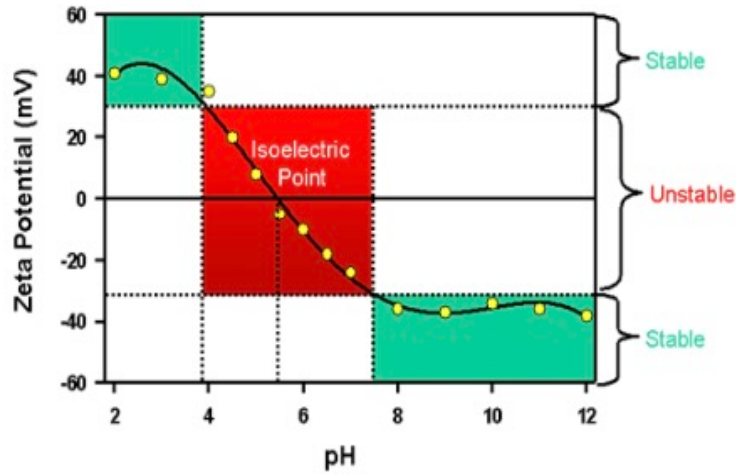


Figure 2.10 Schematic zeta potential Vs pH plot indicating isoelectric point [24]

2.3.5 Focused-Beam Reflectance Measurement (FBRM)

Focused beam reflectance measurement (FBRM) is used to monitor the particle size distribution in situ and agglomerate size in our case. Particle size is an important product specification for many particulate products that should be monitored in line. Therefore, in the past decade, focused beam reflectance measurement (FBRM) has become one of the most frequently used in-line particle characterisation techniques.

The FBRM measurement principle, depicted in Figure 2.11, relies on backward light scattering. To perform the measurement, a laser beam is coupled to an immersible probe via an optical fibre. This laser beam deviated from the probe's central axis with an optical conduit. A rotating lens focuses the laser beam into a dispersed medium, resulting in a double conical laser beam in a circular motion in the medium. When the laser beam intersects with a particle, light is scattered in various directions. [33]. The part of the light scattered back in the incidence angle is collected by the rotating lens. This back-scattered light is coupled via a beam splitter to a second fibre. Through this fibre, the backscattered light is conducted to a detector.

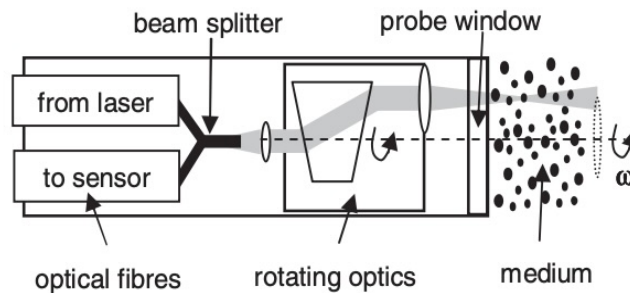


Figure 2.11 Schematic sketch of FBRM probe [33].

By using this measurement principle, chord lengths are recorded as data points. However, it is important to note that even for perfectly spherical particles, a chord length alone does not provide a unique particle size measurement, unlike the diameter, which uniquely defines spheres. To obtain particle size information from the chord length distribution, a model and an inversion algorithm are required. When using the FBRM technique, we typically disperse the agglomerates in water. Dispersion involves the breakdown and distribution of individual particles in a suspension. On the other hand, agglomerates are formed when individual particles or clusters of particles come together and stick to each other, forming clusters. This can occur due to various factors, such as van der Waals.

2.3.6 Inductively Coupled Plasma Spectroscopy (ICP)

Inductively Coupled Plasma (ICP) Spectroscopy is an analytical technique that uses the ionisation of elements present in a sample matrix to measure and identify elements. It finds applications in various surface analysis scenarios, such as the analysis of trace elements, determination of impurities, and characterisation of thin films. It is beneficial for analysing complex samples, as it can provide a high degree of sensitivity and specificity for a wide range of elements. After passing through the ICP, the mass spectrometer separates the ions by their mass-to-charge ratio. The detector then counts the selected ions per second, enabling the instrument to quantify the concentration of each element accurately.

ICP analysis requires liquified sample solutions, so solid samples are often digested prior to analysis. Once the sample is liquid, the ICP aerosolises it with argon (Ar) carrier gas, delivering only the tiniest droplets through the chamber and onto the argon plasma torch. The Ar plasma desolvates and ionises the material, which is subsequently extracted from the plasma using a skimmer, interference cones, and extraction lenses. After passing through the lenses, the ion particles are refined further by an off-axis ion lens, which removes photons and neutral ions and reduces background noise. The ions are separated by their mass-to-charge ratio in the mass spectrometer enabling only the chosen ions to pass on to the detector to be detected and reported by the ICP-MS in terms of counts per second and concentration [34]. ICP analysis can measure the amount of material deposited on the substrate. This information is essential for determining the uniformity and coverage of the coating.

2.3.7 X-Ray Photoelectron Spectroscopy (XPS)

X-ray photoelectron spectroscopy (XPS) is a quantitative technique for determining the elemental composition of a material's surface. It also determines the elemental binding states and typically probes to a depth of 10 nm [35]. The approach is based on measuring the kinetic energy of electrons released from the sample surface when excited by an X-ray source. Electrons are expelled from the innermost shells of the atoms from the sample. Their kinetic energy is determined by the electrons' binding energy, which is unique to each element. The sample's elemental composition can be accurately determined by analysing the X-ray photoelectron spectra.

This analysis for ALD-coated microparticles helps determine the elemental composition of the coating and evaluate the homogeneity of the deposited layer of SiO₂ and TiO₂. It can also offer information on the oxidation state of the elements in the coating, which helps understand the chemical reactions that occur during the ALD process.

2.3.8 Low-Energy Ion Scattering (LEIS)

Low-Energy Ion Scattering (LEIS) is an analytical technique that provides quantitative information on the elemental composition of the outermost atomic layer of the sample. It is the most surface-specific chemical analysis technique of all. In our case, LEIS can be utilized to determine the surface coverage of a thin film or coating on a sample, which is of relevance.

During LEIS analysis, the sample surface is bombarded with noble gas ions of a few keV energy. The energy of the scattered ions reflects the presence of various elements on the surface. This technique can achieve detection limits in the parts-per-million (ppm) range for heavy elements and in the percentage range for light elements. Particles scattered from deeper layers (max. 10nm) contribute to background signals that indicate the presence of elements at those depths. As a result, the element's concentration profile (static depth profiling) is available, providing crucial information such as film thickness. In our study, the experiments were conducted using the IONTOP Double Toroidal Energy Analyser, with Helium ions as the noble gas ions. The incident energy of these ions was set to 3000 eV, and scattering angle at 145°.

3

METHODOLOGY

This chapter describes the methodology that is followed during the course of this project:

3.1 Atomic Layer Deposition

In section 3.1, the details are provided of the materials required (*Expancel*, SiCl_4 , TiCl_4 , H_2O); experimental setup; sample preparation; operating conditions; and sample collection.

3.1.1 Experimental Setup

The flowsheet of the ALD process can be seen in Figure 3.1. The set-up consists of the following parts, where the abbreviations behind the items are given if they are shown in the flowsheet:

- Precursor bubbler with SiCl_4 or TiCl_4 (E-1)
- Oxidizer bubbler with H_2O (E-2)
- Carrier gas flow for precursors (MFC-1)
- Purge gas flow with N_2 (MFC-2)
- Pressure sensor
- Fluidized bed reactor (R-1)
- Back-pulse (V-11)
- Outlet, wash bottles (V-10, F-1, F-2)
- Heating mantle and combined thermocouple
- Thermocouple inside the column
- Vibration table

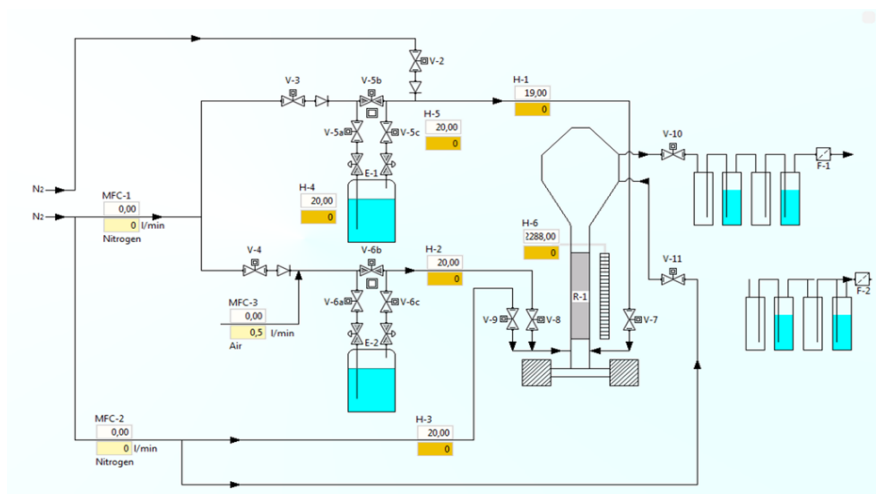


Figure 3.1 Flowsheet of ALD experiment

The entire ALD set-up in the lab is shown in Appendix Figure B.1. The precursor liquids (SiCl_4 , TiCl_4 and H_2O) are located inside the bubblers and are carried with the N_2 gas towards the reactor. The gas enters the fluidized bed reactor from the bottom. The powder bed is fluidized, and the gas exits the reactor at the top. During the process of fluidization, there might be some agglomerates forming in the glass reactor because of the moisture present. These agglomerates can

be broken down to particles' primary size range using the vibrating table, which is usually set at a frequency of 40Hz. The excess precursors and side products are carried off through the outlet towards the wash bottles. The acidic gas HCl, which is a product of the ALD reaction, was neutralized with a base in the wash bottles.

After running the experiments, it was observed that some of the powder was stuck to the wall of the glass, which gave us a decreased amount of powder in the bed. Figure B.2 shows the fluidised bed reactor mounted on a vibrating table, including the heating mantle, which was used for all experiments. The attached thermocouple - 2 can also be seen, which measures the temperature inside the reactor. The heating jacket is attached to the bottom of the column since that is the location of the bed of particles. The temperature of the flow is elevated by using the heating jacket, and the temperature is monitored with two thermocouples. The thermocouple - 2 is located inside the reactor, and the thermocouple - 1 is attached to the surface of the glass column, which acts as a safety limiter and measures the temperature of the heating jacket, and the temperature is generally limited to 60°C. As the reaction is exothermic, the reaction temperature at the bulk would be greater than that of the surface, which will lead the *Expancel* to expand, which is depicted in Figure B.3.

From Figure B.2, we can see that the inlet flow valve and the pressure sensor valve, which is connected to the manometer, are attached to the bottom of the column. The pressure inside the column is monitored with the manometer to avoid over-pressure in the column. If the pressure built up in the system is more than the set pressure, the system trips and automatically shuts down. The reactants are pulsed into the reactor from the bubblers, which are adsorbed on the powder. When the precursor pulse step is over, we purge the system by utilising pure N₂ gas, which will account for the removal of excess reactants or side products formed. The outlet of the reactor, which is present at the top of the column, transports the outlet gas towards the wash bottles. The back pulse valve is also present at the top of the column. After each precursor pulse, a back pulse is carried out to remove possible powder from the distributor plate. This is generally done by closing both valve 9 and valve 11 for a short amount of time while leaving the nitrogen flow (MFC - 2) open. This resulted in a build-up of pressure in the line, and by opening valve 11, the pressure is released from the top of the column. The powder, which was possibly attached to the top distributor plate back, falls back into the column.

3.1.2 Conditions and Parameters

The ALD experiments were performed at a temperature of 50°C and at atmospheric pressure. In order to continuously fluidize the powder, a vibrating table operating at 40 Hz was used at the bottom of the reactor set-up. The precursor was pulsed through the reactor for 45 seconds with a flow velocity of 5 L/min. The purge step duration is 4 mins, depending on flow behaviour. The oxidizer, precursor H₂O, is pulsed for 60 seconds. These values are optimized by previous research on the fluidization of *Expancel*. The precursors that are utilised in the ALD experiments are SiCl₄ and TiCl₄. These precursors are often used in the lab; therefore, the procedure is well-known. It was found that the use of TiCl₄ resulted in better fluidization, meaning that fewer agglomerates were formed. The differences between the two coated powders can be seen in Figures 3.2(a) and 3.2(b).

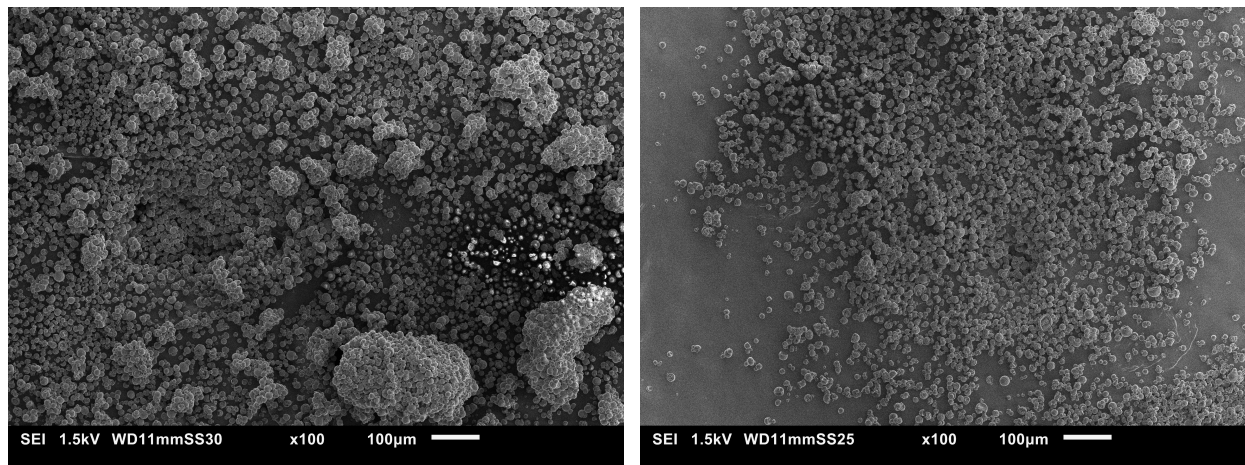


Figure 3.2(a) SEM images depicting the agglomeration of SiO₂ coating.

Figure 3.2(b) SEM images depicting the agglomeration of TiO₂ coating.

Figure 3.2 SEM Images depicting agglomeration of SiO₂ and TiO₂ coating

3.1.3 Collecting The Sample

Collecting the sample was done by disassembling the reactor from the set-up and opening up the bottom. A glass jar was used to collect the coated sample.

3.2 Thermogravimetric Analysis

In section 3.2, the details of the experimental setup, operating conditions and sample preparation are given.

The TGA experiments were carried out on Thermal Analysis System TGA – 2 by Mettler-Toledo GmbH, shown in Figure B.4. In the system, the temperature of a sample is gradually increased while measuring the weight on an analytical balance. In general, the working temperature ranges from 30°C to 1100°C, and the sample is heated at a controlled rate in a specified environment of built-in gas flow control (Air, N₂, CO₂, He, Ar). Then the resulting weight loss is measured, which is due to semi-volatile compounds. TGA is also performed in two stages: isothermal and dynamic. The internal temperature in the system is kept constant during the isothermal stage, while the temperature is increased linearly during the dynamic stage to generate a thermal reaction of the substance. The mass of the sample is continuously monitored during the process to detect changes in the sample. Therefore, as a function of temperature or time, we can obtain and record the change in weight of the substance.

We determined a method to quantify the moisture/water content present on the surface of uncoated and coated samples, which is as follows; the temperature range was set to vary between 25°C and 130°C. The system was set to a temperature of 25°C in an isothermal segment for the first 15 minutes (i.e. temperature was kept constant). Afterwards, the system was transformed into a dynamic segment, in which the temperature was set to climb linearly at a heating rate of 2°C/min until the system reached 130°C. Then the system was immediately turned back into an isothermal segment for 15 minutes. The entire experiment is conducted in N₂ gas, which maintains a dry environment in the apparatus and prevents the sample from absorbing moisture/water content from the atmosphere during the experiment. A very tiny amount of sample from 0.5 mg – 1.00 mg was taken for the analysis. This is because we take the expansion of *Expancel* into consideration. *Expancel* has the tendency to expand when exposed to a temperature greater than 80°C, and this expansion hinders the sensor to monitor the weight loss% of the sample over time.

3.3 Scanning Electron Microscopy

In section 3.3, the details of the experimental setup, operating conditions and sample preparation are given.

Scanning Electron Microscope - Joel JSM - 6010LA was used to determine the surface morphology of the uncoated and coated *Expancel*, as shown in Figure B.5. Carbon tape was placed over the top of a specimen holder to prepare the sample, and a scoop of powder was placed on the carbon tape. The powder was spread out across the surface of the tape with a spatula, and the loose powder was cleared off the surface using an air-pressure bulb. After sample preparation, this specimen holder is mounted into the system. Before the system is evacuated by a vacuum pump, the working diameter is adjusted to ensure better imaging of the sample, which in our case, was adjusted to 10mm. The depth of focus increases as the working distance increases. Following that, the chamber is evacuated to maintain a low vacuum pressure, which is normally between the range of 0.1 - 10⁴ Pa.

The electron gun in SEM typically accelerates electrons through 1 - 30 kV of accelerating voltage, depending on the nature of the specimen. High accelerating voltage enhances electron penetration into the sample, which eventually obscures and blurs the surface features. Thus, keeping the nature of *Expancel* in mind, the accelerating voltage was adjusted between the range of 0.5kV – 5kV.

Another aspect to consider while working with voltages is adjusting the spot size. The spot size can determine the sizes of the sample area from which the signal is produced. The image with a big spot size will be less sharp but smooth, whereas a smaller spot size will result in a sharper but coarser image appearance because of lower signal-to-noise ratios. With high accelerating voltages, the spot size is often considered to be small; however, as the spot size is increased, the accelerating voltage should be lowered. Linear translation (x, y, z), tilt, and rotation modes can all be employed for imaging to modify the position of the specimen in relation to the incoming electron beam.

3.4 Water Contact Angle

In section 3.4, the details of the experimental setup, operating conditions and sample preparation are given.

Contact angles provide information about the hydrophilicity or hydrophobicity of a surface. The Drop Shape Analysis System by Kruss Scientific GmbH was used to measure the Water Contact Angle (WCA), as illustrated in Figure B.7. To determine the contact angle, we must first prepare an appropriate sample. Before performing the WCA experiment, the powder was often pelletised using the die at 1 ton of pressure, as shown in Figure B.6. This was done in order to ensure a smooth surface and reduction of irregularities over the surface. This pelletised sample was then placed over the glass

plate. A syringe of 1mL was entirely filled with demi-water and placed into the system. To avoid inconsistencies in the shape of the water droplet, the glass plate was put directly beneath the syringe. The software Drop Shape Analyser was used to generate a reproducible water droplet with a liquid volume of 5 μ L and a flow velocity of 100 μ L/min. The contact angles were measured immediately after water-tablet contact at room temperature, and the method selected was the sessile drop method.

3.5 Zeta Potential

In section 3.5, the details of the experimental setup, operating conditions and sample preparation are given.

For determining the Zeta Potential, an 100mL of basic stock solution with 40 μ g solid NaOH pellets was prepared in MilliQ water. And the powder concentration to be mixed in the stock solution was taken to be 0.1%, or 1mg/mL, as stated in [36]. The Malvern ZetaSizer Nano series, Nano-ZS, was used to measure the zeta potential. The prepared samples were transferred from glass jars to disposable capillary cells, DTS1070, and then placed in the ZetaSizer. Prior to beginning the experiment, sample specifications had to be determined. The sample material chosen in the Standard Operating Procedure (SOP) was PMMA, with a refractive index of 1.480 and an absorption of 0.010. PMMA is chosen since it is similar to the material of *Expancel*. The dispersant is water, with the default settings. During the experiments, the resulting quality was checked with the Malvern Software. The "Expert Advice" tab within the software was consulted, and if the data did not meet the quality criteria, the sample was checked, and it was run again.

3.6 Focused Beam Reflectance Measurement

In section 3.6, the details of the experimental setup, operating conditions and sample preparation are given.

The focused Beam Reflectance Measurement technique was used to detect the particle agglomeration and phase segregation over time with the help of FBRM G400 by Mettler Toledo, shown in Figure B.9. For FBRM measurement, a solution with an appropriate concentration was prepared in order for the probe to detect the particles in real-time. For the desired concentration, 2 grams of powder was mixed in 200mL MilliQ water, Figure B.8. It is necessary to sonicate the mixture to ensure an equal starting position for each sample. After sonication, the solution is placed onto the magnetic stirrer at 100rpm to maintain steady stirring at room temperature. The probe is inserted into the solution, and we can determine the particle size distribution with respect to time using the software FBRM 4.4.

RESULTS AND DISCUSSION

Atomic Layer Deposition of SiO_2 and TiO_2 was performed over *Expancel* with varying amounts of cycles (C). Our main focus was to prepare the sample with SiO_2 and TiO_2 at 1C, 2C, 3C, 4C, 5C and 10C. These samples were all utilised in the characterisation techniques.

This chapter analyses and discusses the comparative results of uncoated and coated (SiO_2 and TiO_2) particles that are obtained from the performed experiments TGA, SEM, WCA, Zeta Potential, and FBRM mentioned in Chapter 3, and a few other experiments XPS, ICP-EOS and LEIS were not conducted, and the results were provided directly. This chapter starts off with the results obtained from TGA to depict the moisture content present over uncoated and coated micro-particles, followed by the discussion of SEM images that illustrates the surface morphology at different temperatures. Later, the results of the water contact angle and the influence of different coatings on wetting are discussed. An attempt was made to measure the zeta potential and to correlate the results with FBRM measurements. The XPS, ICP and LEIS data provided will be discussed at the end of the chapter.

4.1 Thermogravimetric Analysis

TGA was performed from a temperature range of 25°C to 130°C with a heating rate of 2°C min⁻¹ in the presence of a dry nitrogen environment. Considering the uncoated sample, from the resulting plot in Figure 4.1, the *Expancel* loses weight from the initial stage, i.e. 25°C till onset -1, i.e. 81°C. With the drop in weight% from the temperature of 25°C to 81°C, 97.64% of the initial weight is left, meaning *Expancel* consists of 2.36% of moisture. In Table 4.1, weight loss% from the initial temperature till onset -1, from onset -1 till onset -2, as well as the overall weight loss%, has been depicted for uncoated, SiO_2 and TiO_2 -coated *Expancel*.

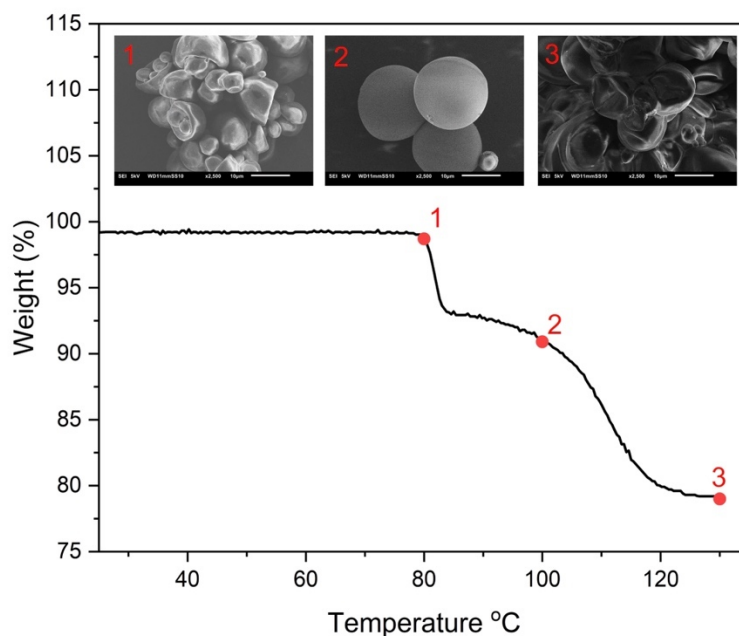


Figure 4.1.1 TGA Plot (Weight% Vs Temperature) for Expancel Uncoated from 25°C – 130°C and SEM images 1, 2, 3 at temperatures 80°C, 100°C, 130°C.

Typically the plot shows the weight change of the uncoated powder as a function of temperature. The initial weight loss in the TGA plot would likely correspond to the removal of any volatile components, such as moisture, from the sample. As the temperature increases from 25°C to 80°C, the plot shows a plateau region where a small amount of deviation in weight% could be observed from the initial state. This could be due to the fact that the sample is directly

exposed to the heat in the TGA system in the dry environment, which results in the elimination of moisture from the surface of the particle.

We can observe from the SEM Image - 1 that there is no major change at the surface of the particle. However, as the temperature continues to increase from 80°C to 84°C, a sudden decrease in weight was observed, which is 4.58%, and after 84°C, a gradual decrease in the weight of the particle was observed. One of the properties of the *Expancel* is that it is thermally stable till 80°C, after this temperature, the particle loses its stability and the gas (iso-butane) encapsulated inside the particle starts to expand (SEM Image - 2), causing the weak spots on the surface to crack, resulting in a decrease in weight with increasing temperature. The overall weight loss% was observed to be 21% of the initial weight.

When analysing *Expancel* coated with SiO₂ and TiO₂ with 10C, a decrease in the weight from the initial stage is observed, as can be seen in Figure 4.1.1. Typically, silica and titania tend to retain moisture, leading to a more significant weight loss compared to uncoated particles. This weight loss can be attributed to the evaporation of moisture from the surface. For SiO₂ 10C, the decrease in weight% from 25°C till 88°C (onset -1) is measured to be 4.24%, while for TiO₂ 10C, the decrease in weight% from 25°C till 82°C (onset - 1) is measured to be 1.49%.

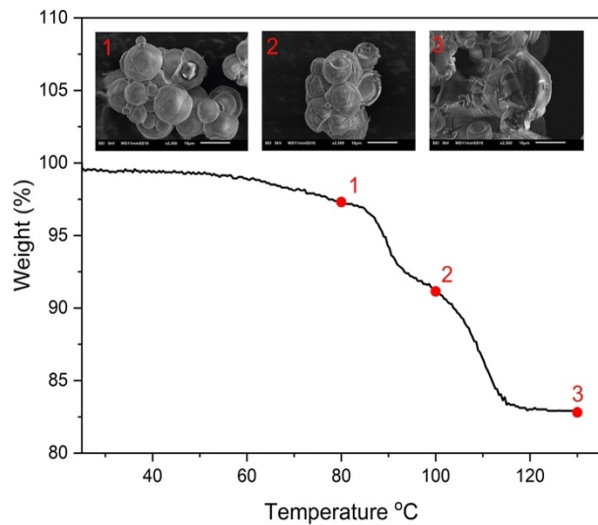


Figure 4.1.2 (a) Weight% Vs Temperature Plot with SiO₂ coating at 10C

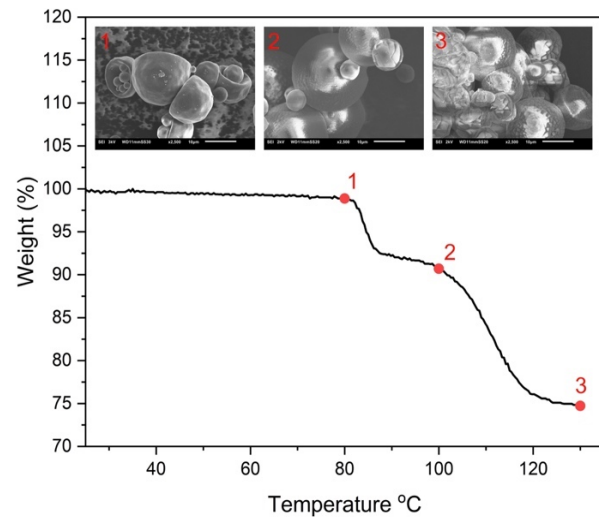


Figure 4.1.2 (b) Weight% Vs Temperature Plot with TiO₂ coating at 10C

Figure 4.1.2 TGA Plot for Expancel from 25°C – 130°C and SEM images 1, 2, 3 at temperatures 80°C, 100°C, 130°C; a) with SiO₂ coating, b) with TiO₂ coating

Considering Figure 4.1.2a, a sudden weight loss from 88°C to 92°C is observed, from which we can state that 3.67% iso-butane was eliminated from the surface within this temperature range. An overall weight loss% from 25°C to 130°C was measured to be 17.19%. Similarly, in Figure 4.1.2b, there is a drastic decrease in weight from 82°C to 87°C, from which we can state that 7.70% isobutane was removed from the surface within this temperature range. And an overall weight loss% from 25°C to 130°C was observed to be 25.53%.

Considering our primary focus on the weight loss percentage from 25°C to onset -1, it can be established that the weight loss % ranges between 2.01 – 4.56% for SiO₂-coated samples, whereas the weight loss% ranges between 1.49 – 6.41% for TiO₂-coated samples. However, no specific trend in the decrease of weight percentage with the increase in coating layers was observed for TiO₂ samples. TiO₂ 3C exhibited a measured weight loss % of 6.41%, which may be a potential error in the sample preparation. On the other hand, for SiO₂ samples, there was an increase in weight loss% from ~2% to ~4%, suggesting an increased affinity with water as the number of coating layers increased.

Samples (with varying no. of cycles)	Initial Temp (°C)	Onset – 1 (°C)	Onset – 2 (°C)	Wt Loss% from Initial Temp till Onset -1 (%)	Wt. Loss% from Onset -1 to Onset -2 (%)	Overall Wt. loss% from 25°C to 130°C (%)
<i>Expancel Uncoated</i>	25	81	84	2.36	4.58	21.00
<i>Expancel SiO₂ 1C</i>	25	83	88	2.01	5.61	24.06
<i>Expancel SiO₂ 2C</i>	25	83	87	2.72	2.71	14.72
<i>Expancel SiO₂ 3C</i>	25	81	86	2.12	4.45	16.82
<i>Expancel SiO₂ 4C</i>	25	81	89	4.56	7.83	30.05
<i>Expancel SiO₂ 5C</i>	25	82	87	3.83	3.50	17.44
<i>Expancel SiO₂ 10C</i>	25	88	92	4.34	3.67	17.19
<i>Expancel TiO₂ 1C</i>	25	80	84	2.93	10.05	33.46
<i>Expancel TiO₂ 2C</i>	25	81	84	1.92	6.80	24.41
<i>Expancel TiO₂ 3C</i>	25	82	85	6.41	8.42	32.86
<i>Expancel TiO₂ 4C</i>	25	81	84	1.99	5.40	19.57
<i>Expancel TiO₂ 5C</i>	25	82	85	2.12	4.84	17.73
<i>Expancel TiO₂ 10C</i>	25	82	87	1.49	7.70	25.53

Table 4.1 Measured TGA data of uncoated, SiO₂ and TiO₂-coated *Expancel* from the initial temperature to onset -1, onset -1 to onset - 2, and overall weight loss%.

4.2 Scanning Electron Microscopy

SEM images of uncoated and coated *Expancel* at varying temperatures (mainly at 80°C, 100°C, and 130°C) were analysed. These temperatures were specified due to the fact that when assessing TGA data, after 80°C, a drastic decrease in weight was observed, and approximately around 100°C, we could observe a gradual decrease in weight till 130°C, after which the weight remained constant. Hence, to evaluate the effect of varying temperatures on *Expancel*, SEM analysis was carried out.

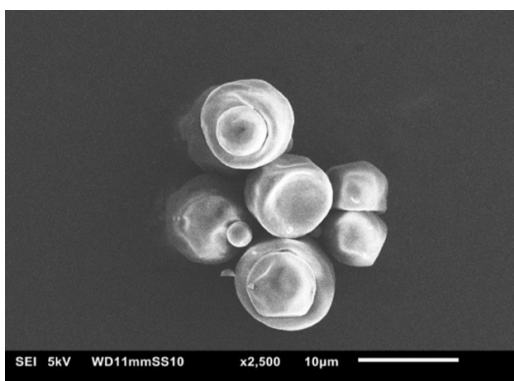
From Figure 4.2a, it can be seen that when *Expancel* was exposed to the temperature of 80°C for 60 min, there was no physical change. At this temperature, it can be assumed that polymer powder is stable (below its glass transition temperature) and can be handled and processed without significant deformation or damage. On the contrary, the microsphere undergoes a physical change when it is heated up to 100°C for 60min. The gas encapsulated inside the particle expands, forming a spherical structure, as seen in Figure 4.2b. This expansion of the gas is facilitated by softening of the polymeric shell. As expansion occurs, the thickness of the polymer shell is decreased drastically, which allows some of the driving gas to escape at this point already. And at a higher temperature of 130°C, the particle expands to its maximum and ruptures causing the gas encapsulated inside the microsphere to escape, as seen in Figure 4.2c. This also explains the constant weight in the TGA plot at 130°C.

Below are the SEM images of SiO₂ 10C coated particles at distinct temperatures. It is evident from the figure that the particles are entirely coated. A substantial thickness and cracking of coating could be observed from these images. However, it is challenging to determine the thickness. When the uncoated particles did not experience any physical change when exposed to the heat at 80°C, it is only logical to not spot any physical changes on the coated particles as indicated in Figure 4.2d. Unlike the uncoated particles, we could not sight a full expansion at 100°C (rupture due to expansion as seen in Figure 4.2e), which could possibly be due to the thick coating that limits the particles from expanding fully. However, it may be worth noting the gaps between the cracks (as opposed to Figure 4.2d, the cracks are completely intact), which might be an indication that the coating ruptured a bit due to the expansion of the particle. This also explains the drop in the TGA curve at this temperature range, the cracks allowing weak spots to be exposed to the heat directly, which eventually leads to the gas to escape which can be measured in terms of weight loss%.

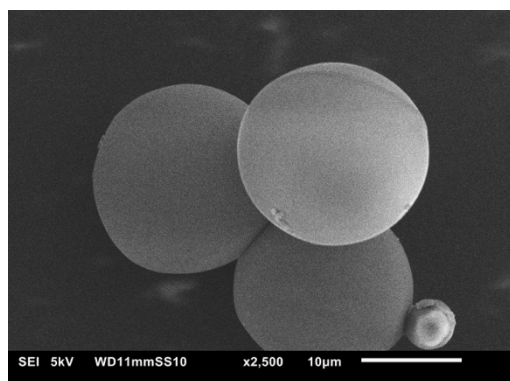
Additionally, it can be observed that at higher temperatures, from 100°C to 130°C, the microsphere undergoes expansion. This results in the particles exceeding in size through the coating, leaving some areas exposed to heat. These exposed areas experience softening of the shell causing weak spots, which eventually leads to the rupture resulting in the distorted coating and the particle as indicated in Figure 4.2f.

Whereas for *Expancel* with TiO₂ 10C coating in Figure 4.2g, we can witness a homogeneous coating without any fractures and no expansion at 80°C. But contrasting to SiO₂ coating at 100°C, we could observe an expansion of the microsphere leading the particles to outgrow the coating. This coating could be seen as fragmented over the surface, which is signified in Figure 4.2h. Additionally, the bright white region can be taken into consideration to have a rough

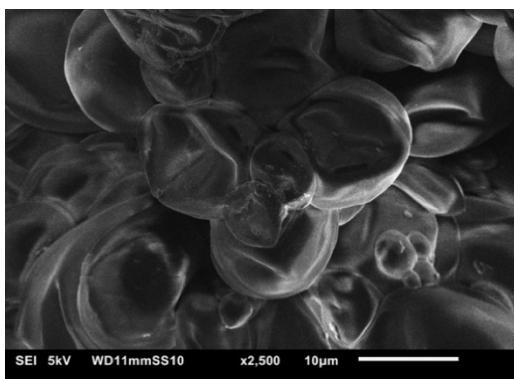
estimate of overcoating in a few regions. And similarly to previous cases at a higher temperature of 130°C, the sphere ruptures (shown in Figure 4.2i).



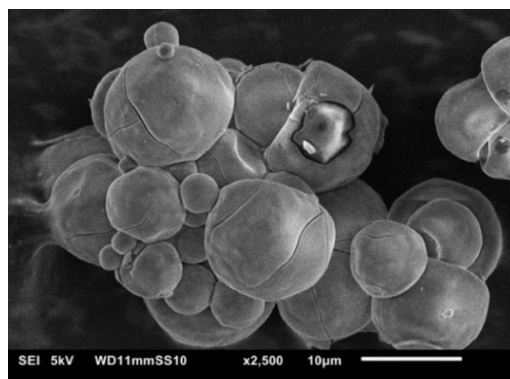
a) *Expancel*/Uncoated at 80°C



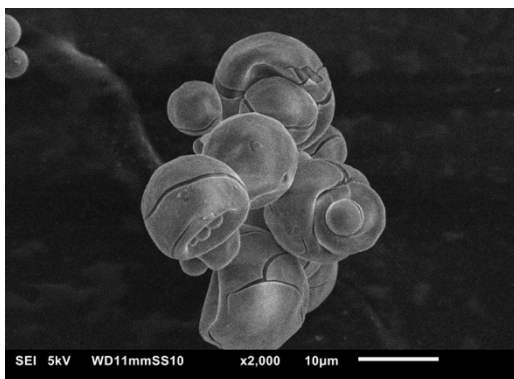
b) *Expancel*/Uncoated at 100°C



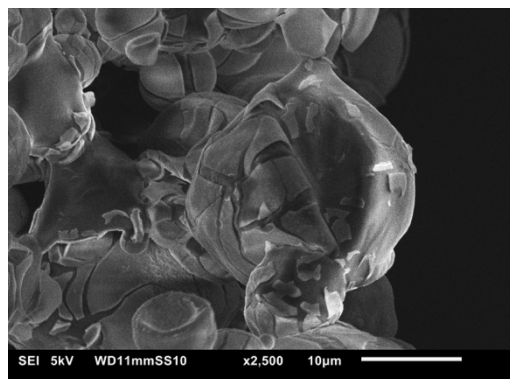
c) *Expancel*/Uncoated at 130°C



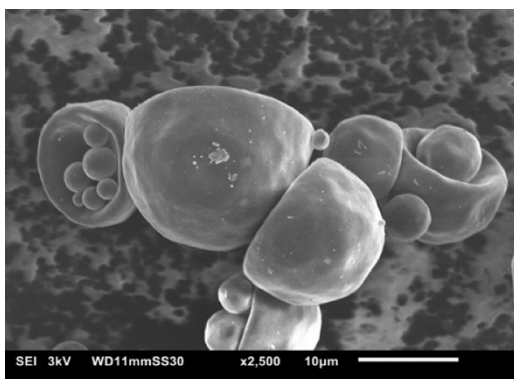
d) *Expancel*/SiO₂ 10C coated at 80°C



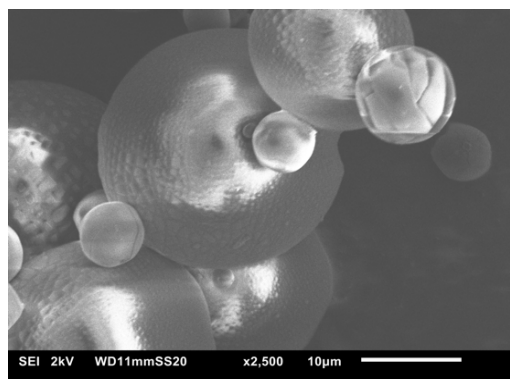
e) *Expancel*/SiO₂ 10C coated at 100°C



f) *Expancel*/SiO₂ 10C coated at 130°C



g) *Expancel*/TiO₂ 10C coated at 80°C



h) *Expancel*/TiO₂ 10C coated at 100°C



i) *Expancel*/TiO₂ 10C coated at 130°C

Figure 4.2 SEM Images of *Expancel* at 2500x with varying temperatures

4.3 Zeta Potential

The results obtained from the zeta potential measurements were deemed inconclusive and, therefore, not discussed in the main report. However, they are presented in Appendix D for reference. When conducting experiments using nanopowders, the influence of gravity and buoyancy can typically be disregarded, and it can be assumed that particle displacement is solely driven by surface interactions. Given the size of our particles, we are operating at the boundary of this assumption's validity, and it is plausible that buoyancy is playing a role. The impact of buoyancy can pose a significant limitation, as the size of the particles increases, the effects of buoyancy forces become more prominent, which causes particles to settle or rise in the solution. This can result in non-reproducible data and pose challenges in accurately interpreting the zeta potential measurements. Zeta Potential measurements would have been advantageous in quantifying the surface charge and having an idea of the agglomerate forming, but due to the limitation, we employed FBRM as an alternate method of measuring the agglomerate forming in real-time in situ.

4.4 Contact Angle Measurements

The primary objective of this project is to quantify the wettability of coated micro-particles which is represented in Figure 4.4. One of the reasons to use SiO₂ and TiO₂ coating over *Expancel* is to improve its wettability, meaning the contact angle should be low, which can be concluded from the data obtained from contact angle measurements. Multiple WCA experiments were performed to quantify the contact angles, and it is evident that the samples coated with SiO₂ have better wettability as compared to TiO₂-coated samples, except for 5C and 10C samples.

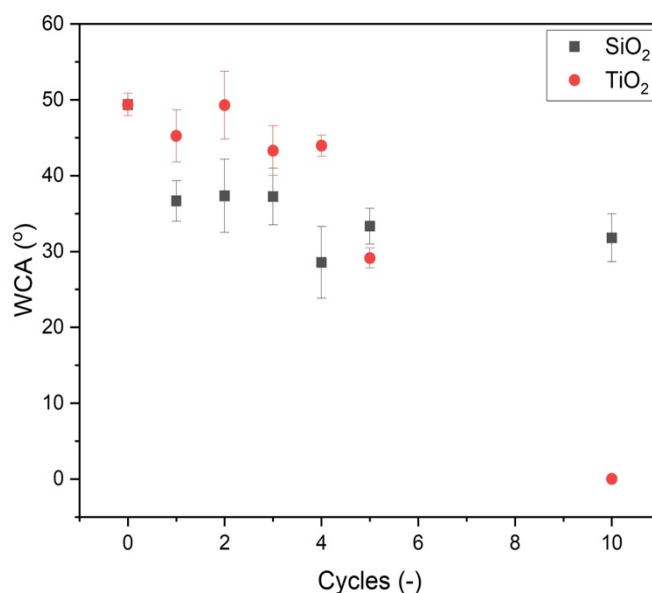


Figure 4.4 Contact angle measurements of uncoated, SiO₂ and TiO₂ coated particles Vs no. of cycles.

The uncoated *Expancel* attained an angle of 49.36°. Thus, in order for us to have better wettability, the coated samples must denote the contact angle lower than the angle formed for the uncoated sample. Therefore, taking into account the water contact angles formed by SiO₂ 1C, 2C, 3C, 4C, 5C, and 10C coated samples were lower than angles formed by uncoated samples. A similar trend was observed for TiO₂ 1C, 2C, 3C, 4C, 5C, and 10C coated samples having lower contact angles. This accomplishes our primary objective of improving wettability.

The SiO₂-coated samples had approximately similar contact angles for 1C, 2C, 3C and 5C. However, for TiO₂-coated samples, except for the 1C sample, a clear trend of decreasing contact angles with increasing no. of cycles was observed. Additionally, for the 10C sample, the contact angle formed was minute, and the software was unable to measure the angle. Thus, the “0” value mentioned in the graph is not measured but inferred from the lack of possibility to measure. The only concerning factor while measuring the contact angles is when pelletising the powder, iso-butane is released from the microspheres, which is adsorbed by the coating, and its presence can influence the water contact angle (WCA). Since iso-butane is hydrophobic, it has the potential to repel water molecules, hindering their spreading and the wetting of the surface. Consequently, this can lead to an increase in WCA and wetting time and may cause deviations from the actual readings when performing the experiments repeatedly.

In general, WCA and wetting time exhibit a complementary relationship where a lower WCA corresponds to shorter wetting times and vice versa. Nevertheless, concerning the wetting time, the average wetting time for uncoated samples was recorded as 88 sec, while the SiO₂ 1C coated sample exhibited a wetting time of 52.74 sec, and the TiO₂ 1C sample demonstrated a wetting time of 50.72 sec. It is worth noting the significant decrease in wetting time of 35.26 sec and 37.28 sec between the uncoated and SiO₂ 1C samples, and the uncoated and TiO₂ 1C samples, respectively (as seen in appendix E. 13). Considering SiO₂-coated samples, except for the 2C sample, there was no significant difference observed thereafter, suggesting that it's just surface coverage which plays the role. On the other hand, wetting time varied among the TiO₂-coated samples. One possible explanation for this variation could be the presence of iso-butane on the coating, which hinders the rapid sinking and complete wetting of the surface by water.

4.5 Focused Beam Reflectance Measurements

This characterization technique was used to analyze the real-time and in situ particle size distribution. One characteristic of *Expancel* is its tendency to form agglomerates upon contact with water. This agglomeration could be attributed to surface charges, prompting the use of FBRM to measure the size of the agglomerates or phase segregation over a period of 60 minutes, with measurements taken every 2sec. While zeta potential measurements could have provided valuable insights into the agglomeration or phase segregation related to surface charges, unfortunately, the obtained data proved inconclusive.

Analysis of the data revealed relatively constant sizes for the formed agglomerates, thus, taking those values into consideration, we obtain the below-mentioned plot of agglomerate size w.r.t varying no. of cycles of coating, as shown in Figure 4.5. The plots incorporate 2 defined parameters, i.e. d₅₀ and d₉₀. The d₅₀ is regarded as the median agglomerate

size indicating that half of the particles in the sample are larger and half are smaller than the defined value. The d_{90} signifies the particle diameter indicating that 90% of the particles in the sample are smaller than the corresponding value. The particle size of *Expancel* typically falls within the range of 12-20 μm . Therefore, it is only logical that the majority of the uncoated, SiO_2 and TiO_2 1C, 2C, 3C, 4C, 5C, and 10C coated particles lie within this size range.

Although, determining whether the agglomerates are formed from smaller particles and increase in size or if the agglomerates are segregated and shifted to the lower size range is challenging. This challenge stems from the limitations of the FBRM probe, which measures the size of particles passing through a laser beam, which means that it is only representative of the particles in that particular location, not taking the bulk into account. This reasoning is applicable to both uncoated and coated particles. Analysing the data for uncoated particles indicates that 90% of the particles are smaller than 70 μm . However, an observation can be made from the raw data of the uncoated samples that the size initially increases, while for the coated samples, the size either decreases or remains stable from the beginning. This strongly suggests that no segregation is occurring as if segregation were present, it would typically lead to a consistent decrease in the measured size.

Figure 4.5 illustrates that as the number of coating layers on particles increases (for SiO_2 1C, 2C, 3C, 5C and TiO_2 1C, 2C, 10C), the formation of larger agglomerates decreases relative to uncoated particles. The reduced agglomerate sizes can be attributed to surface modifications, which bring the surface charge into action upon dissolution in an aqueous solution. The magnitude of the surface charge depends on the pH and ion concentration of the solution, with SiO_2 and TiO_2 particles typically exhibiting a net negative charge at neutral pH [37, 38]. Since the particles tend to have a negative surface charge in an aqueous solution, they repel other negatively charged particles resulting in the segregation of the agglomerates. With coating present, agglomerate sizes may be reduced, but there is no distinct trend, i.e., as the number of coating layers increases, the agglomerate size does not decrease but rather remains nearly equivalent. In Figure 4.5b, TiO_2 3C depicts a distinctive reading, possibly because of the sample preparation error. The new batch for the sample was not prepared due to technical issues with the ALD setup.

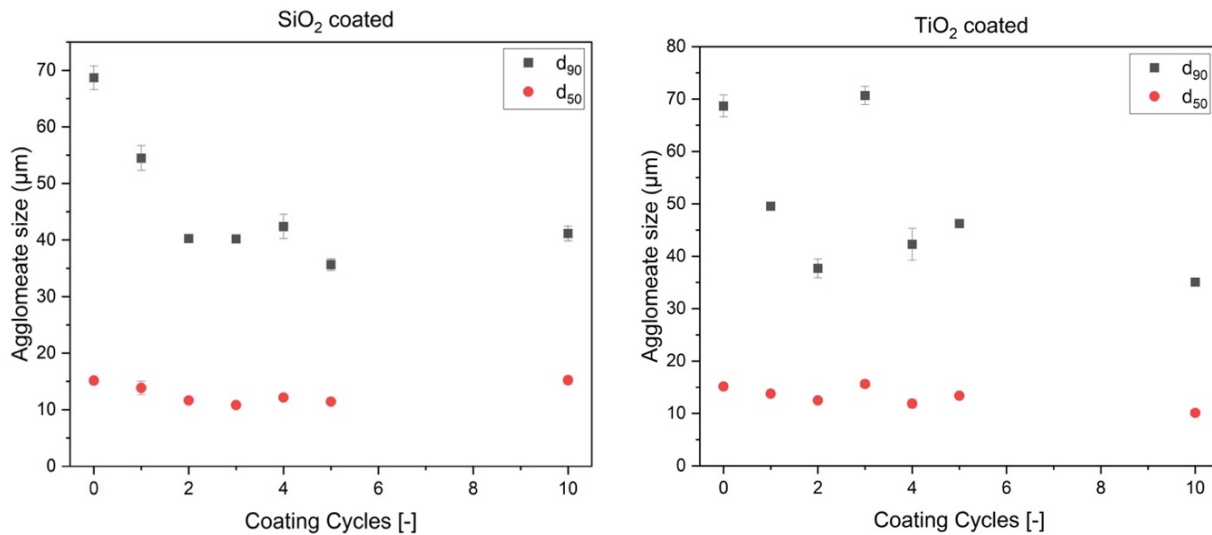


Figure 4.5 (a) Agglomerate size (μm) Vs no of cycles of SiO_2 coated particles Figure 4.5 (b) Agglomerate size (μm) Vs no of cycles of TiO_2 coated particles
 Figure 4.5 FBRM measurement plots indicating the agglomerate size (μm) Vs varying no of cycles.

4.6 X-Ray Photoelectron Spectroscopy

The data for this analysis was provided directly to me. The purpose of utilizing this technique was to determine the elemental composition on the surface of the material. Figure 4.6a represents the atomic percentage of the elements present at the surface w.r.t varying no of cycles for SiO_2 coating. It can be observed from the plot that we do not have the presence of chlorine (Cl) at the surface, which indicates that when sequentially depositing the precursor over the particle, chlorine is completely purged from the system as HCl leaving no trace over the surface.

It is important to consider that XPS has a significant penetration depth that ranges from a few nanometres to tens of nanometres [35]. And *Expancel* is a mixture of acrylonitrile and methyl methacrylate, acrylonitrile is composed of nitrile groups hence N is evident as one of the major elements. Considering the silicon (Si) element, subsequently, we are depositing silica (SiO_2) coating over the particle, it is convincing to detect roughly 20% of Si over the surface. However,

it might be interesting to note that the amount of Si remains consistent with increasing no. of cycles, which basically means that atomic% of Si would nearly be equivalent coating, indicating we do not measure change between 1C coating and 10C. This denotes that we deposit more than 4nm in the first cycle, meaning we measure only the coating in XPS and increasing the thickness of the coating does not alter the detected signal. Though it can be seen in the plot that for 7C, the atomic% for Si decreases, which contradicts expectations and suggests a potential error in sample preparation. When we take Si into account, Oxygen (O) goes concurrently due to the fact that we have SiO₂ as our coating, which is in the ratio 1:2. This means that we observe the atomic% of O present at the surface by exactly 2x the amount of Si, i.e. approximately 40%.

In Figure 4.6b, the graph shows the atomic percentages of elements on the surface as the number of TiO₂ coating cycles varies. SiO₂ has a lower density than TiO₂, which means that the rays will penetrate more deeply into SiO₂ than into TiO₂ for a given energy. This results in a higher probability of detecting deeper layers of SiO₂ with XPS compared to TiO₂. Thus, we obtain 3 – 4% of N when *Expancel* is coated with SiO₂ and for TiO₂ coating a minute amount of N of approximately 2 atomic% at 1C, and it approaches zero with increasing no. of layers. Additionally, the atomic% of Titanium (Ti) is approximately 15 – 17 atomic%, which is lower when compared to the atomic % of Si; but it increases with an increase in coating layers. Generally, the atomic weight of titanium is significantly higher than that of silicon. Due to its heavier atomic weight, the photoelectrons emitted from Ti have lower kinetic energy and thus have a lower probability of being detected by the analyser. However, the presence of other groups (like Cl and C) can also reduce the relative detection of Ti. As a result, a lower atomic percentage of Ti is observed in XPS compared to Si. And for Oxygen (O), when we take Ti into account, O goes concurrently due to the fact that we have TiO₂ as our coating, which is in the ratio 1:2. This means that we observe the atomic% of O present at the surface by exactly 2x the amount of Ti, i.e. approximately 30 – 34%.

In contrast to the SiO₂ coating, which does not contain any chlorine (Cl) groups, the TiO₂ coating exhibits a presence of approximately 3-5 atomic% of Cl. This indicates an incomplete oxidising step during ALD/ CVD process. The presence of Cl on the surface introduces polarity due to its electronegativity, which indicates its stronger attraction for electrons and the creation of a bond based on the electronegativity difference. When water, a polar liquid, comes into contact with a polar surface containing Cl, the partial positive and partial negative charges on both the water molecules and the surface can interact through intermolecular forces. These intermolecular forces facilitate the attractive forces between the liquid and the solid, leading to improved wetting. This explains for the observed trend of progressively lower WCA for TiO₂-coated samples with the increasing no. of layers, whereas SiO₂-coated samples exhibit 38° ± 8° WCA regardless of the number of layers.

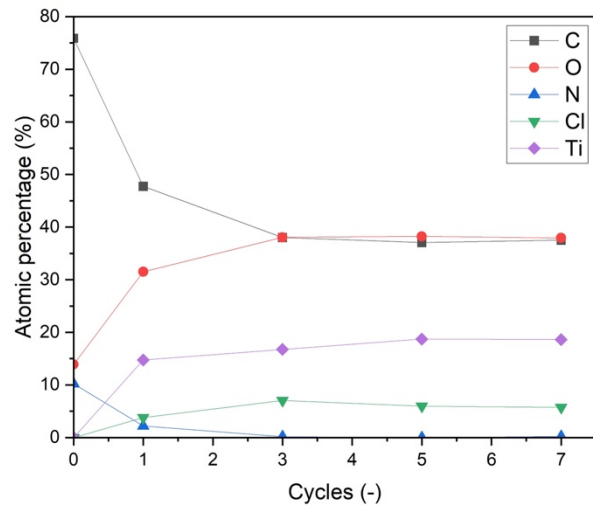
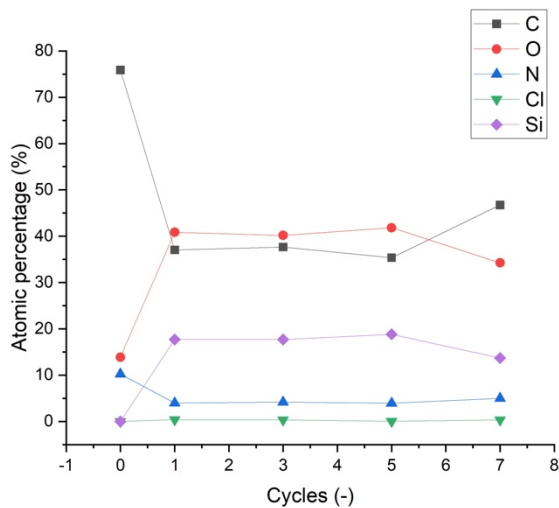


Figure 4.6 (a) Atomic percentage (%) Vs no. of cycles for SiO₂ coating

Figure 4.6 (b) Atomic percentage (%) Vs no. of cycles for TiO₂ coating

Figure 4.6 XPS plot indicating the atomic concentration percentage of different elements Vs varying no. of cycles

4.7 Low Energy Ion Scattering

LEIS is an exquisitely surface-sensitive analytical technique which consists of the bombardment of low-energy noble gas ions over the surface, and the scattered ions are detected in the analyser. In our case, the samples taken into

consideration are uncoated, SiO₂ 1C, 2C, and 100C. Figure 4.7a illustrates the LEIS signal (cts/nC) of scattered ions as a function of the energy.

Typically, LEIS signal Vs Energy plots show a series of peaks corresponding to the energy levels of the different atomic layers in the sample. From the figure below, we may infer that the intensities of Pure SiO₂, SiO₂ 1C, 2C and 100C are identical with the exception of the uncoated samples. Not only the surface peaks but also the overall spectrum shape is identical to bulk SiO₂ powder. The trends in the peak intensities suggest the ALD deposition of SiO₂. The peak, labelled 'Si', remains constant in intensity with the increasing number of deposition cycles, from which we may conclude that there is a full surface coverage of the particle after 1C itself. And after a single ALD cycle, the particle's surface is composed solely of SiO₂, and additional cycles do not alter the composition of the surface.

Since our deposition process exhibits some characteristics of CVD rather than pure ALD, we observe a less conformal coating on the particles. This means that there are variations in the thickness of the coating across the particle, as depicted in Figure 4.7b. In contrast, if it were a "true" ALD process, we would expect to see a highly conformal coating without such variations. The SEM image of the SiO₂ 1C sample, in which we can observe sputtered patches deposited over the particle, confirms the presence of CVD behaviour. It can also be inferred that the particle is fully covered, and the sputtered effect may be attributed to the excess deposition of SiO₂. Consequently, we can estimate that the coating after 1C is relatively thick compared to what would be achieved in a "true" ALD process. Thus, the lack of variation in the peaks for SiO₂ 1C, 2C and 100C could indicate that the deposition process is not effectively modifying the composition of the SiO₂ coating with increasing cycles.

And since we are coating SiO₂, which is in the ratio of 1:2, the peaks for Oxygen (O) are double those of Si peaks.

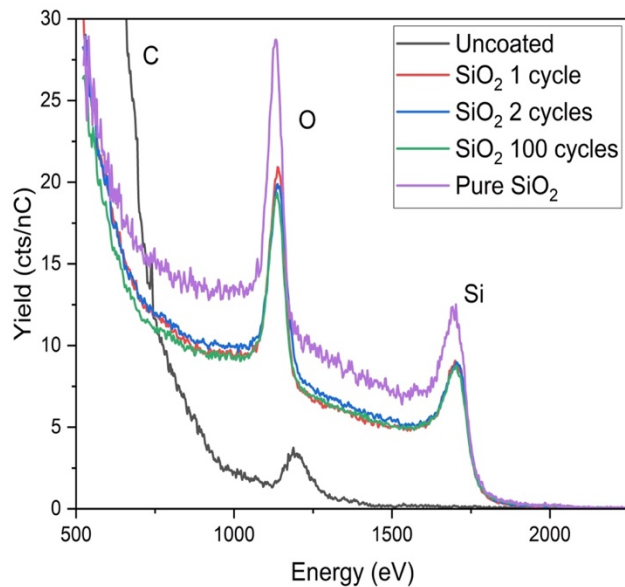


Figure 4.7(a) Energy(eV) Vs Yield (cts/nC) plot of uncoated, coated samples

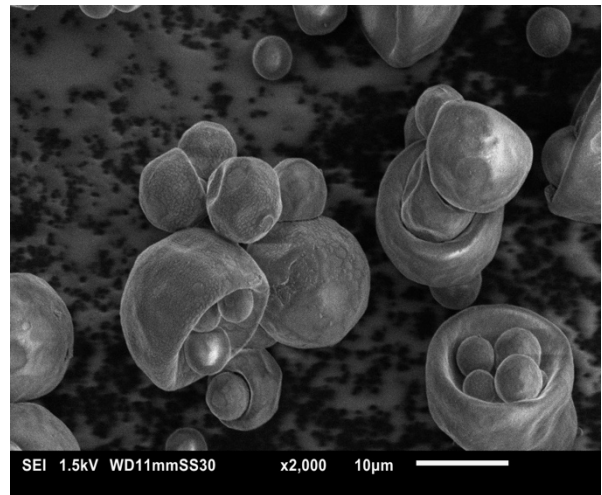


Figure 4.7 (b) SEM image of SiO₂ 1C sample denoting CVD behaviour

Figure 4.7 LEIS spectra for uncoated and SiO₂ 1C, 2C and 100C coated microparticle and SEM Image of SiO₂ 1C sample

4.8 Inductively Coupled Plasma

ICP is a bulk analytical technique that can provide information about the elemental composition of a sample as a whole, including the concentration of trace elements. This analytical technique was taken into consideration to determine the amount of silicon and titanium elements present in the coating over the particle. To accurately measure the weight percentage of silicon, the SiO₂ coating needed to be dissolved in an acidic solution, and SiO₂ can certainly be dissolved in the acids, which would provide us with reliable data that implies the weight% of silicon [39].

From Figure 4.8 below (note the double y-axis; the black colour axis on the left side represents Ti (wt%) and the red colour axis on the right side represents Si (wt%) with varying cycles (x-axis)), we can roughly estimate the weight% with varying no. of cycles. For SiO₂ 1C, Si present is approximately 5.2 – 5.3 wt%, for SiO₂ 2C, Si present is 6 wt%, for SiO₂ 3C, Si present is approximately 3.7 – 3.8 wt%, for SiO₂ 4C, Si present is 7 wt%, for SiO₂ 5C, Si present is 5 wt%, for SiO₂ 10C, Si present is approximately 5.8 wt%, and for SiO₂ 100C, Si present is 8 wt% which is understandable as for 100C, the SiO₂ deposited over the particle is a lot. Considering that our deposition process exhibits CVD behaviour, the increased

weight percentage of silicon on the particles can be justified. In "true" ALD, we would expect to see a smaller amount of weight% instead of this observed increase. This observation could be supported by the XPS results, which indicate that the layer deposited after the first cycle exceeds the thickness of 4nm, whereas, in theory, a thickness of approximately 0.2nm is to be expected. However, based on the provided data, we cannot discern any specific trends in the weight percentage with an increasing number of cycles.

It is important to note that the data provided for TiO₂ may not be as reliable. In general, TiO₂ is more challenging to dissolve for ICP analysis compared to SiO₂. This is because TiO₂ has a higher melting point and is more resistant to acid attack than SiO₂. Thus for TiO₂ 1C, Ti present is approximately 0.2 – 0.3 wt%, for TiO₂ 2C, Ti present is 0.5 wt%, for TiO₂ 3C, Ti present is 0.4 wt%, for TiO₂ 4C, Ti present is 0.6 wt%, for TiO₂ 5C, Ti present is 0.75 wt%, for TiO₂ 10C, Ti present is approximately 1.3 wt%, and for TiO₂ 100C, Ti present is 2 wt%. Unlike silicon, which showed inconsistent trends, we can observe a general trend of increasing titanium content with an increasing number of cycles, except for the TiO₂ 3C-coated samples. It is possible that this discrepancy in the TiO₂ 3C data could be attributed to errors during sample preparation, although the exact reason cannot be determined.

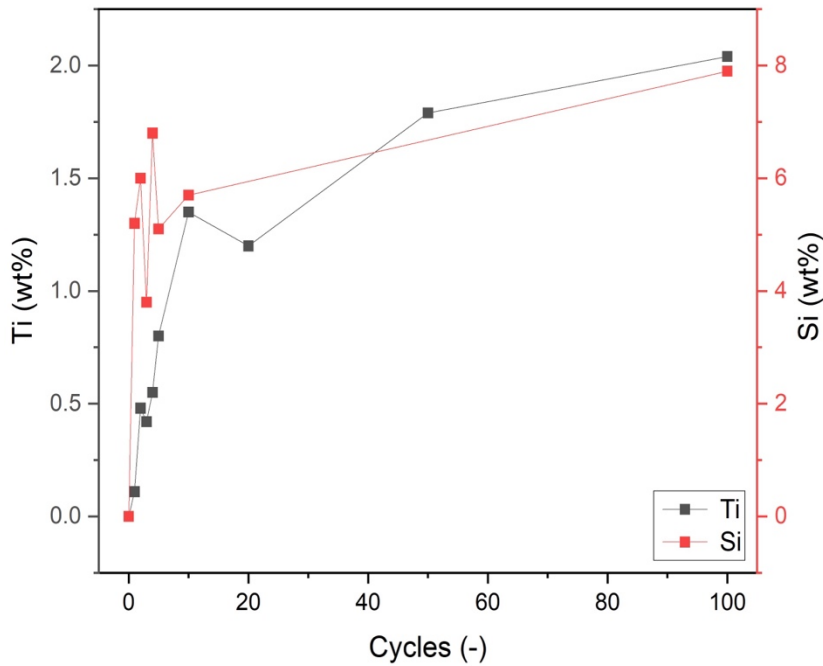


Figure 4.8 Plot for ICP denoting weight% of titanium and silicon w.r.t varying no. of cycles

CONCLUSION AND RECOMMENDATION

It was determined that *Expancel* lacks affinity with water thus, to enhance its affinity with water, hydrophilic compounds such as SiO₂ and TiO₂ were used as coatings using atomic layer deposition. It was established that using SiO₂ and TiO₂ as coating improved the wettability of *Expancel*.

TGA was used to examine the water affinity by exposing the particles to heat directly in the temperature range of 25°C – 130°C under inert conditions. In TGA, however, it is assumed that the initial weight loss is due to the elimination of moisture from the surface based on the reasoning that the coated microparticles are directly exposed to the heat under inert conditions, i.e. in a dry environment. Our primary focus was to measure the weight loss% from the initial stage, i.e. 25°C till 80°C (onset - 1), which denotes the weight loss% due to loss of moisture from the surface. From the analysis, it can be established that the weight loss % ranges between 2.01 – 4.56% for SiO₂-coated samples, whereas the weight loss% ranges between 1.49 – 6.41% for TiO₂-coated samples. However, no specific trend in the decrease of weight percentage with the increase in coating layers was observed for TiO₂ samples. On the other hand, for SiO₂ samples, there was an increase in weight loss% from ~2% to ~4%, suggesting an increased affinity with water as the number of coating layers increased. However, currently, we are unaware of any other volatile components discharging from the surface till the Onset - 2. Thus, a recommendation for future research to strengthen our reasoning, evolved gas analysis could be considered to analyse explicitly which components are evolved during this particular temperature range.

To study the surface morphology of coated particles at different temperatures, 80°C, 100°C, and 130°C. SEM Analysis was performed. In general, it was observed that till 80°C, there was no expansion observed for the microparticles, whereas, at 100°C, we could observe a full expansion of the particles. At 130°C, the particles were observed to be ruptured due to the fact that, after full expansion, the gas encapsulated into the particle is completely escaped.

To quantify the wettability of coated particles, Water Contact Angles (WCA) were measured. A comparison was made between uncoated, SiO₂ and TiO₂-coated particles. The data indicated that the wettability of *Expancel* was improved. Through WCA, reduced contact angles for coated particles were observed, signifying enhanced wetting. For the wetting time, the average wetting time for uncoated samples was recorded as 75.73 sec, while the SiO₂ 1C coated sample exhibited a wetting time of 52.74 sec, and the TiO₂ 1C sample demonstrated a wetting time of 50.72 sec. It is worth noting the significant decrease in wetting time of 22.99 sec and 25.01 sec between the uncoated and SiO₂ 1C samples, and the uncoated and TiO₂ 1C samples, respectively. Considering SiO₂-coated samples, except for the 2C sample, there was no significant difference observed thereafter, suggesting that it's just surface coverage which plays the role. On the other hand, wetting time varied among the TiO₂-coated samples. For contact angle measurements, we require to pelletise the powder under high pressure, which resulted in the discharge of iso-butane that can be observed in the liquid phase when pelletising the uncoated powder. However, when pelletising the coated powder, iso-butane is not been seen. This is because iso-butane gets absorbed into the coating, which might hamper the contact angle measurements and wetting time. This is merely a hypothesis and has not been substantiated as a proven fact. Pelletising the coated samples can induce cracks due to the mechanical stress applied to it, and this changes surface roughness as well as revealing some of the substrate underneath the coated surface, which is also an important parameter in determining the WCA. Therefore, it is also recommended to quantify the surface roughness.

Zeta potential measurements were inconclusive for our case. It would have been advantageous in quantifying the surface charge and understanding the agglomeration or segregation, but due to the large particle size, it is assumed that the buoyancy is playing a role in causing the particles to freely move into the cuvette during the measurement, because of this limitation, we employed FBRM as an alternate method of measuring the agglomerate forming in real-time in situ. Considering the *Expancel* particle size, i.e. 12-20 µm range, and the property of forming an agglomerate when it comes in contact with water, these agglomerates may cause inconsistent data; thus it is recommended to sonicate the solution before measuring the zeta potential.

Since the particle tends to agglomerate upon contact with water, it is essential to quantify the surface charge. To assess this, zeta potential and FBRM measurements were used. For Zeta Potential measurements, the data obtained were insignificant, which was due to the fact that the particles formed an agglomerate that eventually had an effect on buoyancy, causing the particle to move in the cuvette, which disrupted our data. So, it is recommended that after preparing the solution of coated powder and the NaOH solution, the solution needs to be sonicated in order for the

agglomerate particles to break into the primary size range, which may not interfere with the zeta potential measurements.

From the FBRM measurements, the agglomerate size as a function of time was measured for coated particles with varying deposition layers. The coated particles exhibited reduced agglomerate sizes when compared to the uncoated particles. However, the TiO₂ 3C coated sample indicated the agglomerate size ($d_{90} \sim 72 - 73 \mu\text{m}$), which is greater than the uncoated samples, which is not expected and might be due to the error in the sample preparation. To assess the consistency and observe any potential trends, it is recommended to prepare a fresh batch of TiO₂ 3C-coated samples to gather a new dataset. This will enable us to verify if a consistent pattern is being followed. These coated particles possess surface charges at the surface, which cause the agglomeration or segregation of the particles. For FBRM measurements, we used MilliQ water (pH 7) to prepare the mixture. However, to understand the agglomeration and segregation of the particles due to surface charges, we can correlate these surface charges data which are obtained from zeta potential. For successful correlation, it is recommended to prepare the mixture for FBRM and zeta potential at the same pH.

Furthermore, through XPS data analysis, we were able to identify the elemental compositions present on the surface when the particle is coated with varying numbers of layers. This analysis revealed that silicon (Si) is present in higher concentrations compared to titanium (Ti). ICP provided us with the weight % of Si and Ti. However, it is important to note that the weight percentage of Ti obtained from ICP analysis may not be entirely reliable. This is because ICP analysis requires the elements to be dissolved in an acidic solution, but Ti is not readily soluble in acidic mediums, leading to potentially inaccurate results. For Si, the data implied that the amount of Si present on the surface is a lot more than the expected theoretical value as we are not performing 'true' ALD, thus we have CVD behaviour in the reactor. And from LEIS, we were able to determine that after depositing one layer of coating (1C), we achieved full surface coverage and thick coating, indicating that the particle's surface is primarily composed of SiO₂. Increasing coating cycles did not significantly alter the composition of the surface.

REFERENCES

1. Expancel Overview Brochure: Nouryon; <https://www.nouryon.com/globalassets/inriver/resources/brochure-expancel-the-engineered-solution-global-en.pdf>
2. Puurunen, R. L. (2005). Surface chemistry of atomic layer deposition: A case study for the trimethylaluminum/water process. *Journal of Applied Physics*, 97(12), 121301. <https://doi.org/10.1063/1.1940727>
3. Putkonen, M., & Niinistö, L. (2005). Organometallic Precursors for Atomic Layer Deposition. *Springer-Verlag EBooks*, 125–145. <https://doi.org/10.1007/b136145>
4. George, S. Z. (2010). Atomic Layer Deposition: An Overview. *Chemical Reviews*, 110(1), 111–131. <https://doi.org/10.1021/cr900056b>
5. Zara, D. L., Zhang, F., Sun, F., Bailey, M. R., Quayle, M. J., Petersson, G., Folestad, S. & van Ommen, J. R. (2021, maart). Drug powders with tunable wettability by atomic and molecular layer deposition: From highly hydrophilic to superhydrophobic. *Applied Materials Today*, 22, 100945. <https://doi.org/10.1016/j.apmt.2021.100945>
6. “The Processes Used to Deposit Nano-Scale Coatings.” [Online]. Available: <https://www.forgenano.com/processes-used-deposit-nano-scale-coatings-sol-gel-co-precipitation-cvd-ald-ald/>
7. Puurunen, R. L. (2003). Growth Per Cycle in Atomic Layer Deposition: A Theoretical Model. *Chemical Vapor Deposition*, 9(5), 249–257. <https://doi.org/10.1002/cvde.200306265>
8. Weimer, A. W. (2019). Particle atomic layer deposition. *Journal of Nanoparticle Research*, 21(1). <https://doi.org/10.1007/s11051-018-4442-9>
9. “The Processes Used to Deposit Nano-Scale Coatings.” [Online]. Available: <https://www.forgenano.com/processes-used-deposit-nano-scale-coatings-sol-gel-co-precipitation-cvd-ald-ald/>
10. C.A.Bishop (2011), “Atomic Layer Deposition,” *Vacuum Deposition onto Webs, Films and Foils*, pp. 331–336, [Online]. Available: <https://linkinghub.elsevier.com/retrieve/pii/B978143778670000192>
11. Richey, N. E., De Paula, C., & Bent, S. F. (2020). Understanding chemical and physical mechanisms in atomic layer deposition. *Journal of Chemical Physics*, 152(4), 040902. <https://doi.org/10.1063/1.5133390>
12. Ommen, J. R., Goulas, A. & Puurunen, R. L. (2021, 16 september). Atomic Layer Deposition. *Kirk-Othmer Encyclopedia of Chemical Technology*, 1–42. <https://doi.org/10.1002/0471238961.koe00059>
13. Knez, M., Nielsch, K., & Niinistö, L. (2007b). Synthesis and Surface Engineering of Complex Nanostructures by Atomic Layer Deposition. *Advanced Materials*, 19(21), 3425–3438. <https://doi.org/10.1002/adma.200700079>
14. Puurunen, R. L., & Vandervorst, W. (2004). Island growth as a growth mode in atomic layer deposition: A phenomenological model. *Journal of Applied Physics*, 96(12), 7686–7695. <https://doi.org/10.1063/1.1810193>
15. Feng, L. (2018). *Application of Atomic Layer Deposition on Ceramic Nanofiltration Membrane*. TU Delft Repositories. <https://repository.tudelft.nl/islandora/object/uuid%3Ab80c338e-5de8-4eb8-a4f1-15af96cbdec0>
16. Mallik, A. K., Chisty, A. H., Kabir, S. F., Khan, M. I., Haque, P., & Rahman, M. M. (2022). Coating of chitosan onto bone implants. *Elsevier EBooks*, 355–381. <https://doi.org/10.1016/b978-0-12-821058-1.00001-0>
17. Dillingham, G. (2022, October 14). *What is a Contact Angle?* Retrieved October 19, 2022, from <https://www.brighton-science.com/what-is-contact-angle>
18. Tran, P. A., & Webster, T. J. (2013). Understanding the wetting properties of nanostructured selenium coatings: the role of nanostructured surface roughness and air-pocket formation. *International Journal of Nanomedicine*, 2001. <https://doi.org/10.2147/ijn.s42970>
19. PerkinElmer. (n.d.). TGA beginners guide. *Resources PerkinElmer*. https://resources.perkinelmer.com/corporate/cmsresources/images/44-74556gde_tgabeginnersguide.pdf

20. Editorial Board. (2022, December 12). Scanning Electron Microscope (SEM) - Diagram, Working Principle, Components and Cost. *Microscope Wiki*. <https://microscopewiki.com/scanning-electron-microscope/>
21. Goodhew, P. J., Humphreys, J., & Humphreys, J. (2000). Electron Microscopy and Analysis. *CRC Press EBooks*. <https://doi.org/10.1201/9781482289343>
22. ST Instruments. (n.d.). *Overcoming charge-up effects in scanning electron microscope*. <https://www.stinstruments.com/materials-science/overcoming-charge-up-effects-in-scanning-electron-microscopes-sems/>
23. Varenne, F., Botton, J., Merlet, C., Vachon, J., Geiger, S., Infante, I. C., Chehimi, M. M., & Vauthier, C. (2015). Standardization and validation of a protocol of zeta potential measurements by electrophoretic light scattering for nanomaterial characterization. *Colloids and Surfaces A: Physicochemical and Engineering Aspects*, *486*, 218–231. <https://doi.org/10.1016/j.colsurfa.2015.08.044>
24. Colorado State University. (n.d.). *Zeta potential - An introduction in 30 minutes*. <https://www.research.colostate.edu/wp-content/uploads/2018/11/ZetaPotential-Introduction-in-30min-Malvern.pdf>
25. Hiremath, P. G., Rajashekhara, S., Binnal, P., & Theodore, T. (2021). Fluoride Contamination in Underground Water and Its Treatment. *Elsevier EBooks*, 249–280. <https://doi.org/10.1016/b978-0-12-822263-8.00009-9>
26. Kirby, B., & Hasselbrink, E. F. (2004). Zeta potential of microfluidic substrates: 2. Data for polymers. *Electrophoresis*, *25*(2), 203–213. <https://doi.org/10.1002/elps.200305755>
27. Kemell, M., Färm, E., Ritala, M., & Leskelä, M. (2008). Surface modification of thermoplastics by atomic layer deposition of Al₂O₃ and TiO₂ thin films. *European Polymer Journal*, *44*(11), 3564–3570. <https://doi.org/10.1016/j.eurpolymj.2008.09.005>
28. Zhang, D., La Zara, D., Quayle, M., Petersson, G., Van Ommen, J. R., & Folestad, S. (2019). Nanoengineering of Crystal and Amorphous Surfaces of Pharmaceutical Particles for Biomedical Applications. *ACS Applied Bio Materials*, *2*(4), 1518–1530. <https://doi.org/10.1021/acsabm.8b00805>
29. Zhang, D., Quayle, M., Petersson, G., Van Ommen, J. R., & Folestad, S. (2017). Atomic scale surface engineering of micro- to nano-sized pharmaceutical particles for drug delivery applications. *Nanoscale*, *9*(32), 11410–11417. <https://doi.org/10.1039/c7nr03261g>
30. Abdulagatov, A. I., Orudzhev, F., Rabadanov, M. K., & Abdulagatov, I. M. (2016). Copper nanowire arrays surface wettability control using atomic layer deposition of TiO₂. *Russian Journal of Applied Chemistry*. <https://doi.org/10.1134/s1070427216080085>
31. Ding, Y., Xu, S., Zhang, Y., Wang, A. C., Wang, M. E., Xiu, Y., Wong, C., & Wang, Z. L. (2008). Modifying the anti-wetting property of butterfly wings and water strider legs by atomic layer deposition coating: surface materials versus geometry. *Nanotechnology*, *19*(35), 355708. <https://doi.org/10.1088/0957-4484>
32. Shimel, M., Gouzman, I., Grossman, E., Barkay, Z., Katz, S., Bolker, A., Eliaz, N., & Verker, R. (2018). Enhancement of Wetting and Mechanical Properties of UHMWPE-Based Composites through Alumina Atomic Layer Deposition. *Advanced Materials Interfaces*, *5*(14), 1800295. <https://doi.org/10.1002/admi.201800295>
33. Kail, N., Briesen, H., & Marquardt, W. (2007b). Advanced Geometrical Modeling of Focused Beam Reflectance Measurements (FBRM). *Particle & Particle Systems Characterization*. <https://doi.org/10.1002/ppsc.200601036>
34. *ICP-MS as a Technique / OHSU*. (n.d.). <https://www.ohsu.edu/elemental-analysis-core/icp-ms-technique>
35. Mather, R. (2009). Surface modification of textiles by plasma treatments. *Elsevier EBooks*, 296–317. <https://doi.org/10.1533/9781845696689.296>
36. Van Dam, J. F. K. (2022). *Relating Nano-coating Thickness to Stability of Powder In Water*. Delft University of Technology.
37. Xu, P., Wang, H., Tong, R., Du, Q., & Zhong, W. (2006). Preparation and morphology of SiO₂/PMMA nanohybrids by microemulsion polymerization. *Colloid and Polymer Science*, *284*(7), 755–762. <https://doi.org/10.1007/s00396-005-1428-9>
38. Thevenot, P., Cho, J. Y., Wavhal, D., Timmons, R. B., & Tang, L. (2008). Surface chemistry influences cancer killing effect of TiO₂ nanoparticles. *Nanomedicine: Nanotechnology, Biology and Medicine*, *4*(3), 226–236. <https://doi.org/10.1016/j.nano.2008.04.001>

39. Bossert, D. E., Urban, D. A., Maceroni, M., Ackermann-Hirschi, L., Haeni, L., Yajan, P., Spuch-Calvar, M., Rothen-Rutishauser, B., Rodriguez-Lorenzo, L., Petri-Fink, A., & Schwab, F. (2019). A hydrofluoric acid-free method to dissolve and quantify silica nanoparticles in aqueous and solid matrices. *Scientific Reports*, 9(1). <https://doi.org/10.1038/s41598-019-44128-z>

APPENDICES



USER MANUALS

A.1 Experimental Procedure

The stepwise procedures for the experiments performed are stated below.

A.1.1 Atomic Layer Deposition

1. Preparing the reactor
 - Take the supplies (distributor plates, rubber seals, wind boxes) and glass column out of the oven and put them in the fumehood
 - Take 2 clamps; and a thermocouple
 - Take *Expancel* and place it in the fumehood
 - Take the sieves that are suitable according to the particle size
 - Put metal granules in the top and middle sieves
 - Put approximately 3 scoops of Expancel into the top sieve with the help of a spatula
 - Cover the sieves with a plastic bag
 - Place the sieve on the vibrating plate for 10 min
2. In the meantime, prepare the bottom and top of the reactor
 - Take the distributor plate and wrap it with teflon tape
 - After wrapping, fit the distributor plates into the wind box
 - Attach the lower part to the reactor, use the clamp for this
 - When the sieve is ready, collect the powder in a beaker
 - Pour the powder into the reactor using the funnel
 - Now, put the upper part on the reactor and secure it with the clamp
 - Put the thermocouple in the reactor through the bottom nozzle on the side. Twist the rubber, do not push.
 - Also, put a rubber on the top spot, again turn, don't push
 - The reactor is now ready to go for ALD
3. Preparing the ALD
 - Get the wrench + Allen key
 - Place the reactor in the holders and tighten it slightly
 - Attach the output, back pulse, and input
 - Attach the thermocouple to the electric socket
 - Check for the leakages
 - Load your program into the PC
 - Run the program.
 - Turn on the vibrating plate
 -

A.1.2 Thermogravimetric Analysis

1. Preparing the sample
 - Take out the crucible from the TGA machine
 - Place it in the weighing balance
 - With the help of a spatula, place the powder into the crucible until it weighs **0.5 – 0.7mg**
 - Place the crucible into the TGA machine
2. Defining the method
 - Select the N_2 condition
 - Set the initial temperature at **25°C**
 - Set the end temperature at **130°C**

- Set the **static** segment for **20min** at the initial and end temperatures
 - Set the **dynamic** segment with a heating rate of **2°C min⁻¹**
3. After defining the method, start the experiment
 - Enter the details in the pop-up (i.e. weight of the sample, weight of the crucible)

A.1.3 Water Contact Angle

1. Preparing sample
 - The powder is pelletised using a die
 - The sample holder is fitted at the bottom of the die
 - The powder is placed onto the sample holder
 - Another sample holder is placed at the top of the powder
 - The die is placed into the palletizer, and close the lid
 - The pressure is set to 1ton
 - Hit the start button to apply the pressure for roughly **10 -15sec**
 - After, gently remove the pelletised sample and place it in the sample box
2. Setting up the contact angle machine
 - Take a syringe and rinse it with demi water
 - After washing, fill the syringe with water till 1mL
 - Place the syringe at the syringe holder and tighten the knob
 - Place a slide at the bottom of the syringe
3. WCA
 - Open the software Drop Shape Analyser
 - For **dosing**, adjust the plunger using the arrows
 - Put the setting in **continuous mode** and adjust the rate to **1000µL**
 - Hit the arrow and wait till the bar hits its max limit
 - After, select the setting to **volume**
 - Set the liquid volume to **5µL** and rate at **100µL** and press the arrow to start
 - From **option**, select the drop type to **sessile drop**
4. To acquire the image
 - Open FG Drop window
 - Click the 'Acquire' icon
 - Adjust the focal length and magnification of the camera
 - Set illuminating strength to **12-13**, brightness to **163**, and contrast to **127**
 -
5. For Results
 - After dosing, press the water contact icon
 - In the **result window**, measure the contact angles

A.1.4 Scanning Electron Microscopy

1. Preparing sample
 - Make sure to wear gloves when touching the sample
 - Take a sample holder and carbon tape
 - Put the tape on the sample holder
 - Place a tiny amount of powder onto the sample holder
 - Blow Nitrogen on your sample to remove loose particles
2. SEM
 - Open software – Joel JSM
 - The SEM machine is always on with a vacuum, so press **VENT** to shut down the motors
 - After the motors are shut, check for the pop-up notification on the computer
 - Open the machine and adjust the height of the machine with the help of z-axis to 10mm
 - Place the sample in it
 - Close the machine
 - Press **EVAC** in the software and push the door to seal
3. For Imaging
 - Hit the **ON** option (present at the top) for the beam to start
 - Start with the default setting, Signal – **SEI**, voltage with **5kV**, WD with **10mm**, SS with **50**
 - Adjust the focus and magnification

A.1.5 Focused Beam Reflectance Measurement

1. Preparing the solution
 - Weigh **2mg** of powder
 - Take **200ml** of **MilliQ** water in a beaker
 - Mix the powder into the water thoroughly
 - Cover the beaker with paraffin film
 - **Sonicate** the solution for **10 - 15min**
2. FBRM
 - Open the software FBRM 4.4
 - Select New Experiment
 - Take 200ml of MilliQ water in a beaker
 - Switch on the probe
 - Put the probe in the MilliQ water (after putting the probe into the water, the line that appears on the screen indicates the particle size)
 - If the line is **red**, clean the probe with ethylene/acetone, and put the probe again in the MilliQ water till the line is indicated in **green**
 - After, put the probe immediately into the solution (don't let the probe hit the stirrer or the breaker), and place it steady with the help of the clamp
 - Place the beaker onto the magnetic stirrer
 - Set the stirring rate to **100rpm**

A.1.6 Zeta Potential

1. For sample preparation
 - Prepare a **100mL** stock solution with **40µg** NaOH pellet in MilliQ water
 - Mix the required powder (SiO₂ or TiO₂ coated samples) into the solution
 - Sonicate for **10 - 15mins**
 - Transfer the solution into the cuvette with the help of syringe
 - Put the cuvette in the Zetasizer
2. For measuring the Zeta Potential
 - Run the application as "**Admin**"
 - Click on '**New Experiments**'
 - Define parameters (Cuvette – DTS 1070, SOP – PMMA, Refractive Index – 1.480, absorption – 0.010, dispersant - water)

B

EXPERIMENTAL SETUP

The below-mentioned Figure B.1 shows the experimental setup of ALD in the lab. The key things are indicated with the 'yellow' arrow.

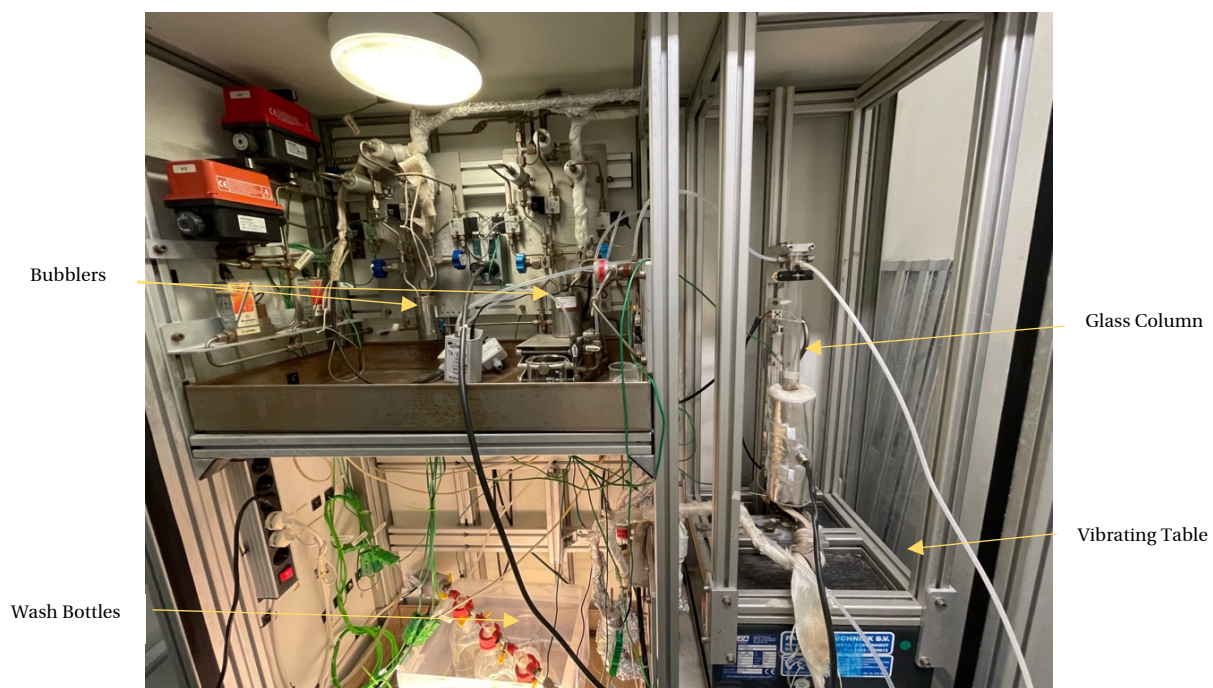


Figure B. 1 ALD experimental set-up in the lab

The below-mentioned Figure B.2 shows the fluidised bed reactor mounted on a vibrating table.

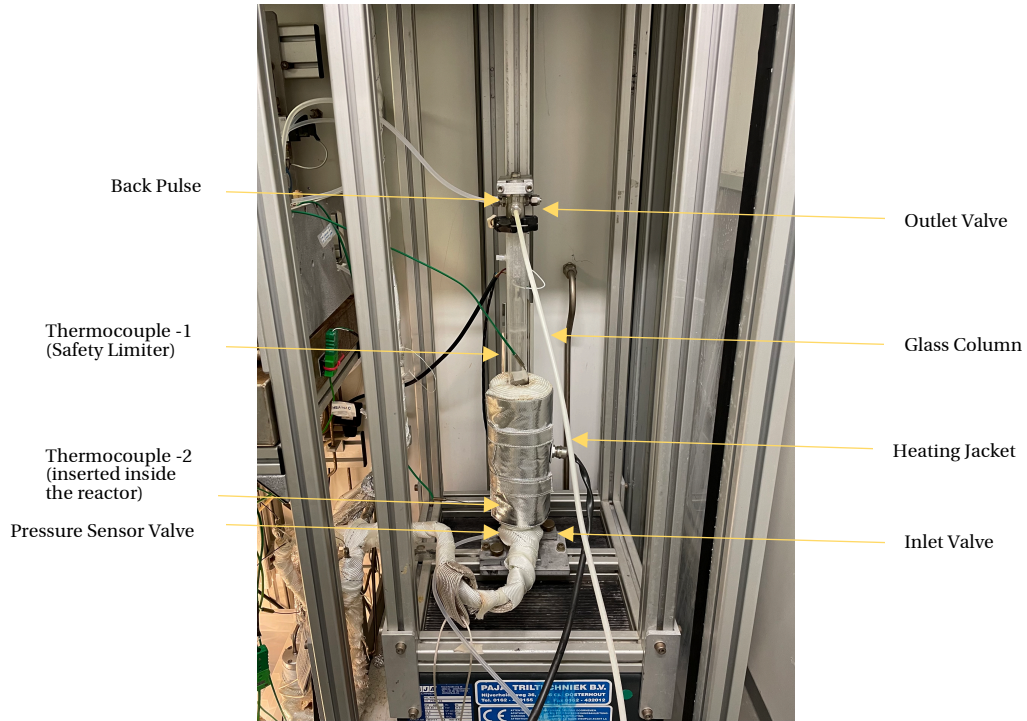


Figure B.2 Fluidised bed reactor mounted on a vibrating table

The below-mentioned Figure B.3 shows the expansion of *Expancel* in the reactor due to exothermic reaction.



Figure B.3 Expanded Expancel due to exothermic reaction

The below-mentioned Figure B.4 shows the TGA machine present in the Spectroscopy Lab.

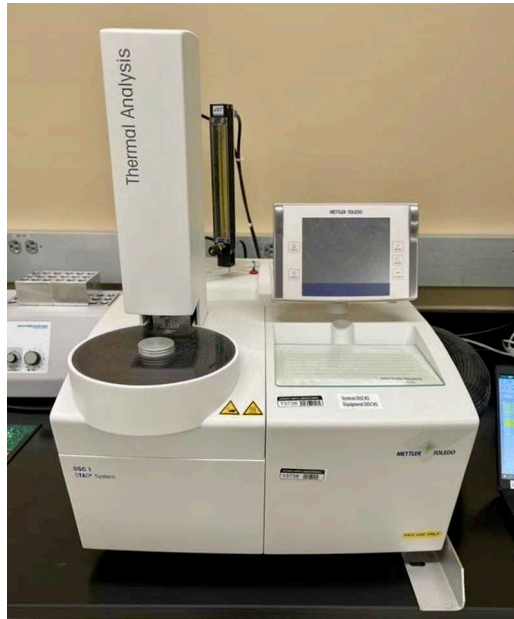


Figure B. 4 Thermal Analysis System TGA – 2 by Mettler-Toledo GmbH

The below-mentioned Figure B.5 shows the SEM machine present in the SEM Lab.



Figure B. 5 Scanning Electron Microscope – Joel JSM – 6010LA

The below-mentioned Figure B.6 shows the powder pelletising die for WCA, and Figure B.7 shows the experimental setup for contact angle measurements in chemical synthesis lab.



Figure B. 6 Power Pelletising die

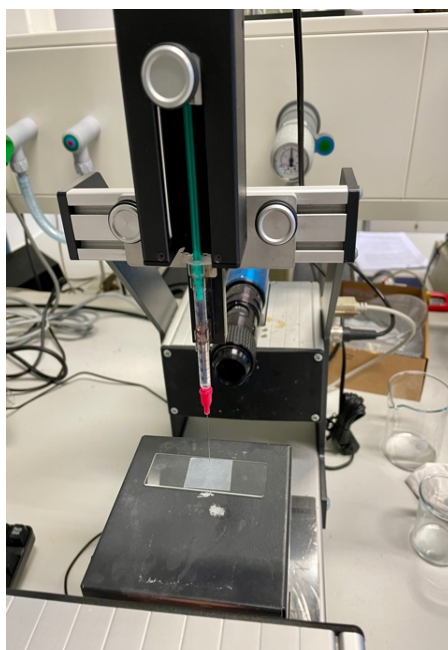


Figure B. 7 Experimental setup for measuring WCA

The below-mentioned Figure B.8 shows the mixture of *Expancel* mixed in water for FBRM measurements, and Figure B.9 shows the experimental setup for FBRM present in 3Me.

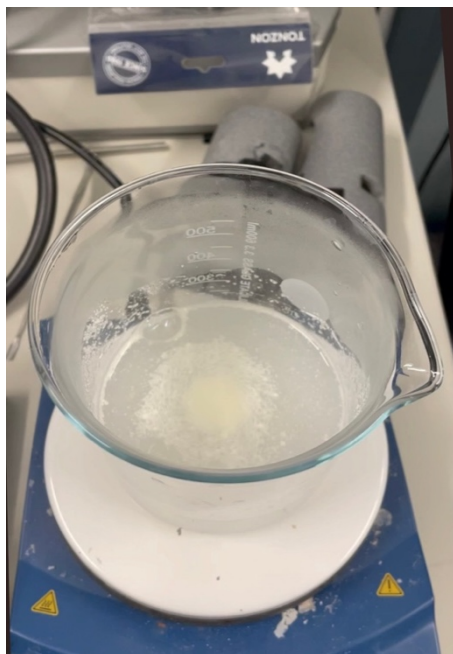


Figure B. 8 Power Mixed in 200mL MilliQ water

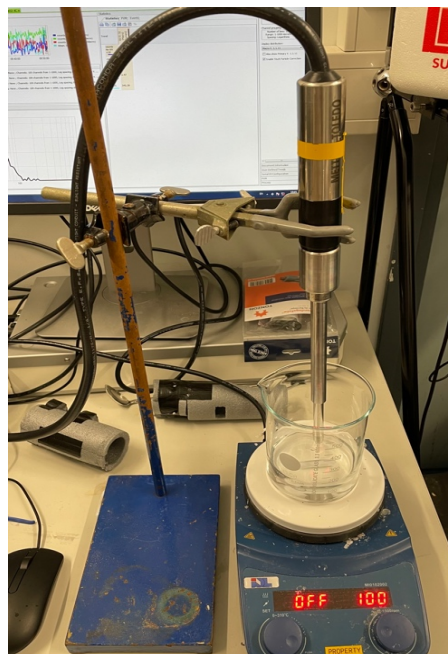


Figure B. 9 Experimental setup of FBRM

C

CONTACT ANGLE MEASUREMENTS

The Table C.1 denotes WCA for specific samples with their standard deviations.

Samples (With Varying No. Of Cycles)	WCA (°)	Standard Deviation
<i>Expancel Uncoated</i>	49.36	1.31
<i>Expancel SiO₂ 1C</i>	36.5	2.66
<i>Expancel SiO₂ 2C</i>	37.34	4.83
<i>Expancel SiO₂ 3C</i>	37.25	3.74
<i>Expancel SiO₂ 4C</i>	28.56	4.73
<i>Expancel SiO₂ 5C</i>	37.25	3.74
<i>Expancel SiO₂ 10C</i>	31.8	3.14
<i>Expancel TiO₂ 1C</i>	45.24	3.43
<i>Expancel TiO₂ 2C</i>	49.28	4.46
<i>Expancel TiO₂ 3C</i>	43.3	3.27
<i>Expancel TiO₂ 4C</i>	43.93	1.39
<i>Expancel TiO₂ 5C</i>	29.13	1.31
<i>Expancel TiO₂ 10C</i>	0	0

Table C.1 Measured water contact angle (WCA) of uncoated, SiO₂ and TiO₂-coated *Expancel*

D

ZETA POTENTIAL DISTRIBUTION

Below mentioned are the zeta potential distributions for the uncoated, SiO₂ and TiO₂ 1C, 2C, 3C, 4C, 5C, and 10C coated samples.

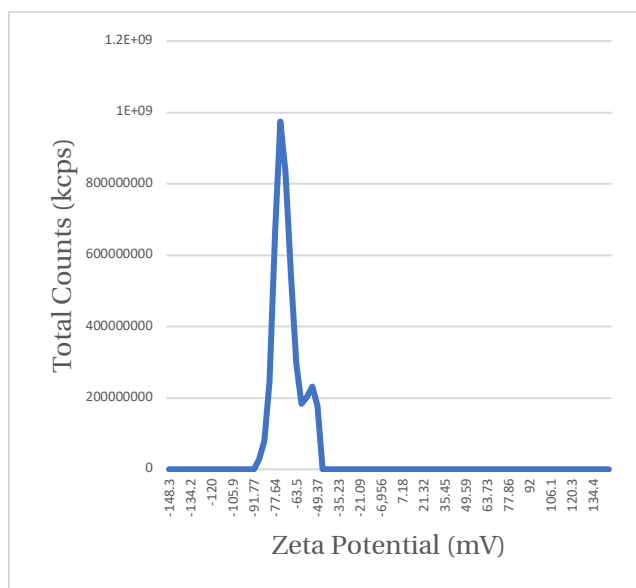


Figure D.1 Zeta Potential (mV) Vs total counts(kcps) for uncoated sample

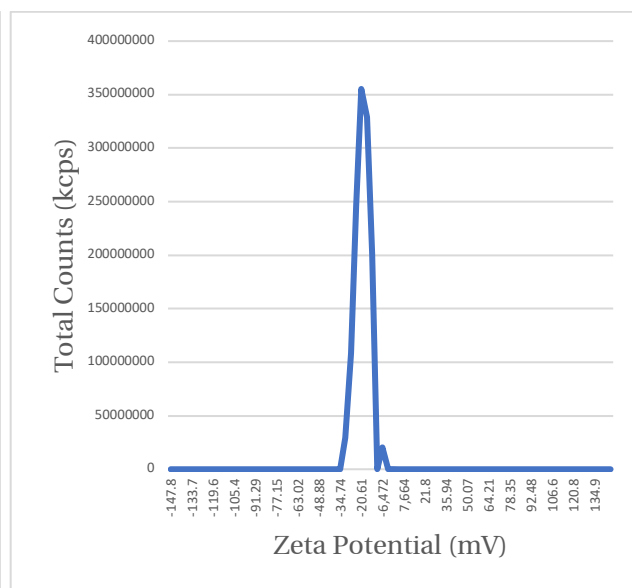


Figure D.2 Zeta Potential (mV) Vs total counts(kcps) for SiO₂ 1C sample

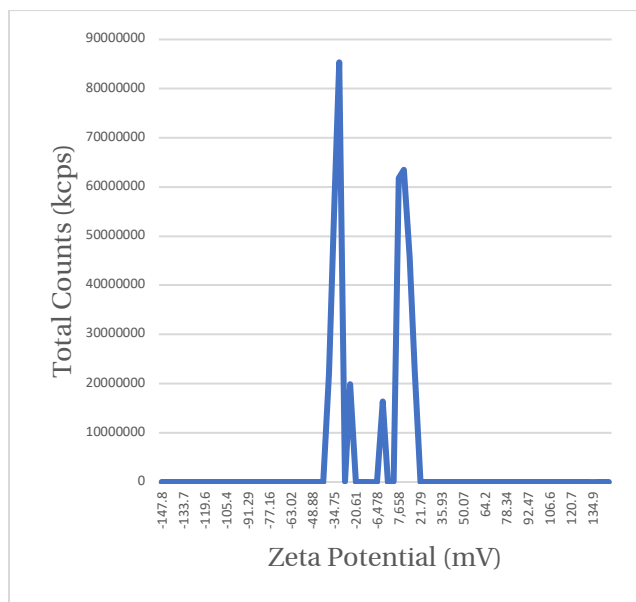


Figure D.3 Zeta Potential (mV) Vs total counts(kcps) for SiO₂ 2C sample

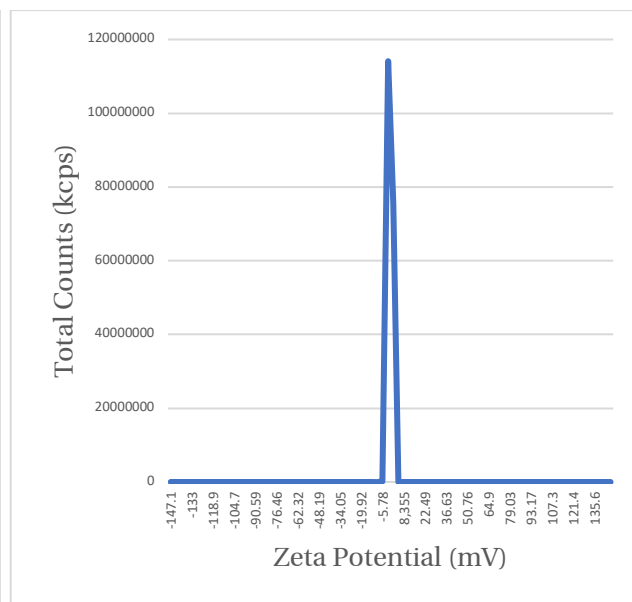


Figure D.4 Zeta Potential (mV) Vs total counts(kcps) for SiO₂ 3C sample

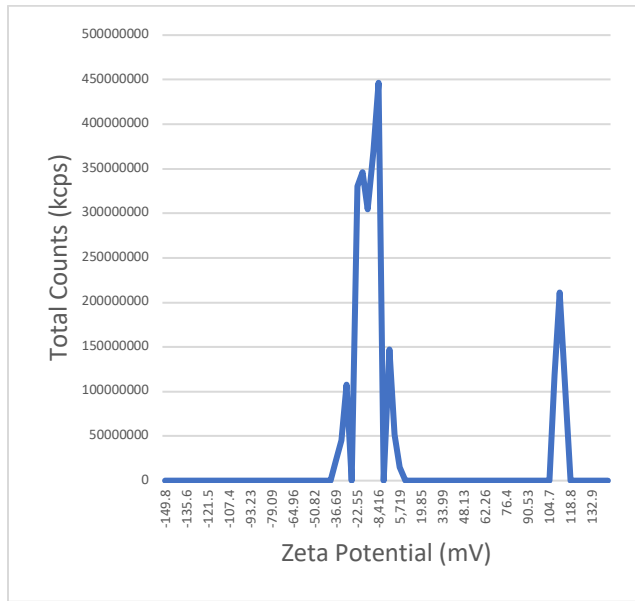


Figure D.5 Zeta Potential (mV) Vs total counts(kcps) for SiO₂ 4C sample

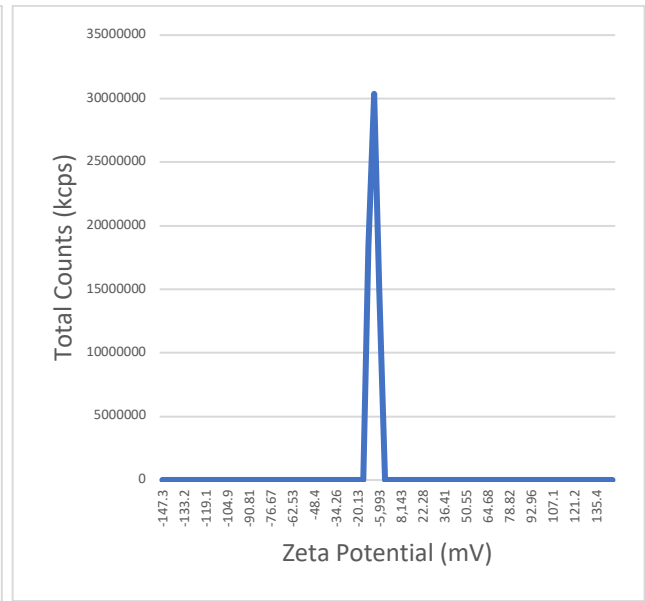


Figure D.6 Zeta Potential (mV) Vs total counts(kcps) for SiO₂ 5C sample

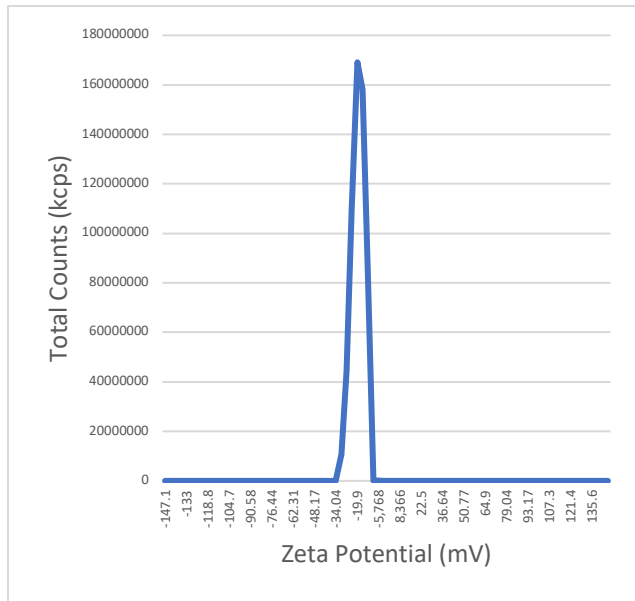


Figure D.7 Zeta Potential (mV) Vs total counts(kcps) for SiO₂ 10C sample.

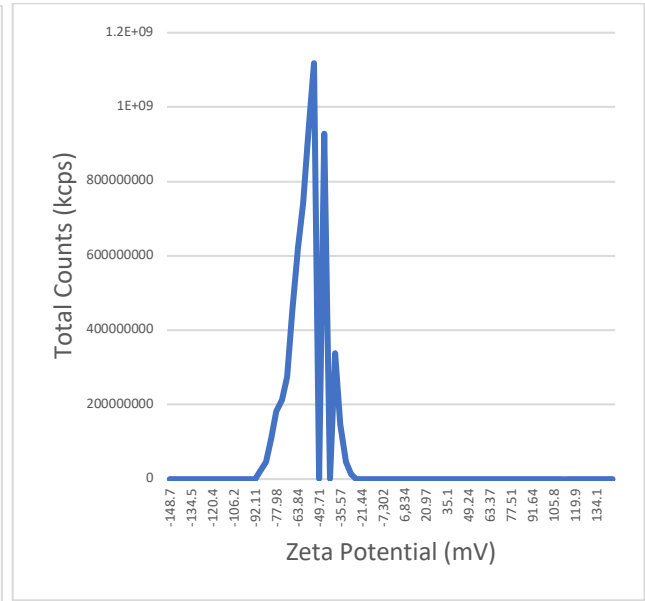


Figure D.8 Zeta Potential (mV) Vs total counts(kcps) for TiO₂ 1C sample

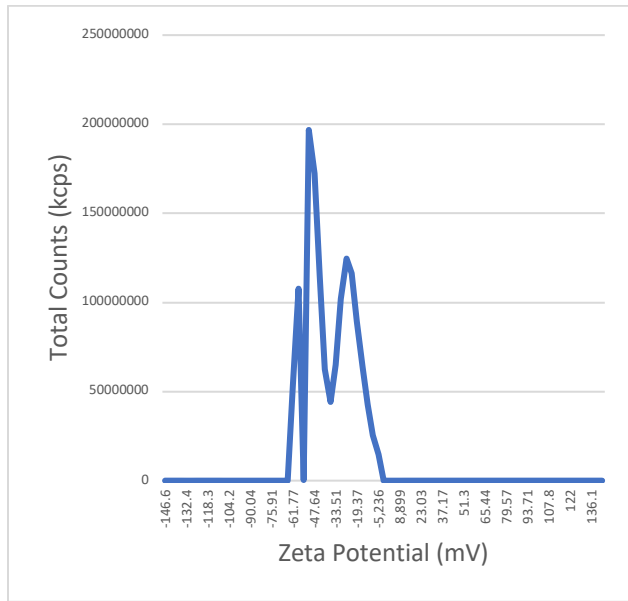


Figure D.9 Zeta Potential (mV) Vs total counts(kcps) for TiO₂.2C sample.

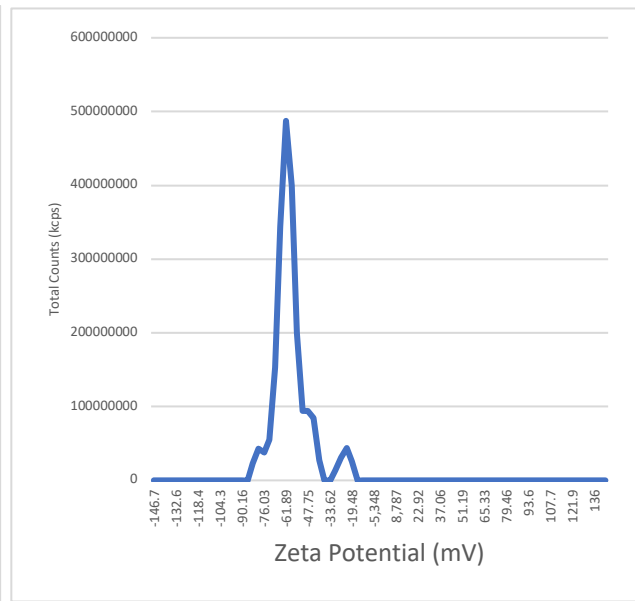


Figure D.10 Zeta Potential (mV) Vs total counts(kcps) for TiO₂.3C sample

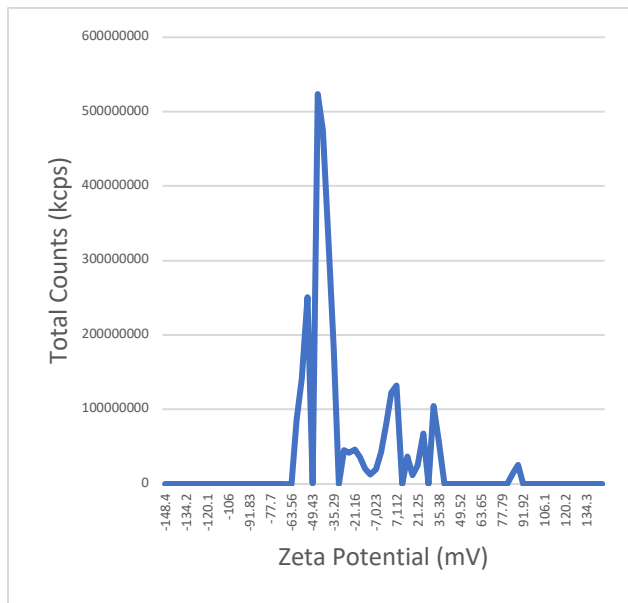


Figure D.11 Zeta Potential (mV) Vs total counts(kcps) for TiO₂.4C sample.

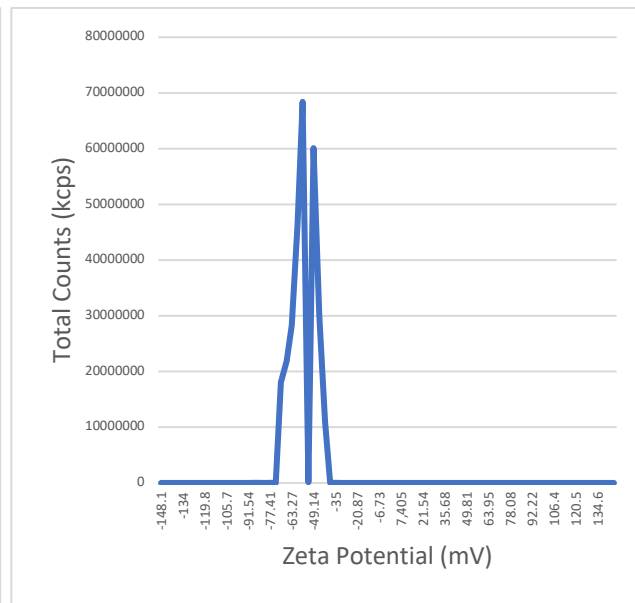


Figure D.12 Zeta Potential (mV) Vs total counts(kcps) for TiO₂.5C sample

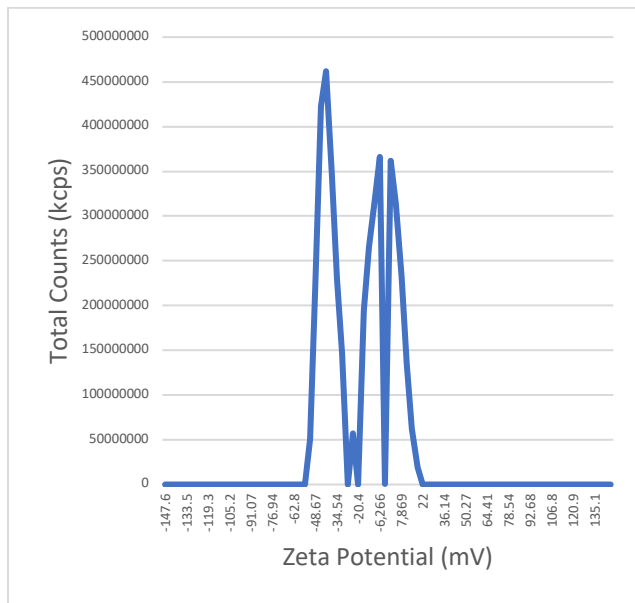


Figure D.13 Zeta Potential (mV) Vs total counts(kcps) for TiO₂ 10C sample

E

WETTING TIME

The recorded wetting time plots (Wetting Time Vs No. of Attempts) are mentioned below:

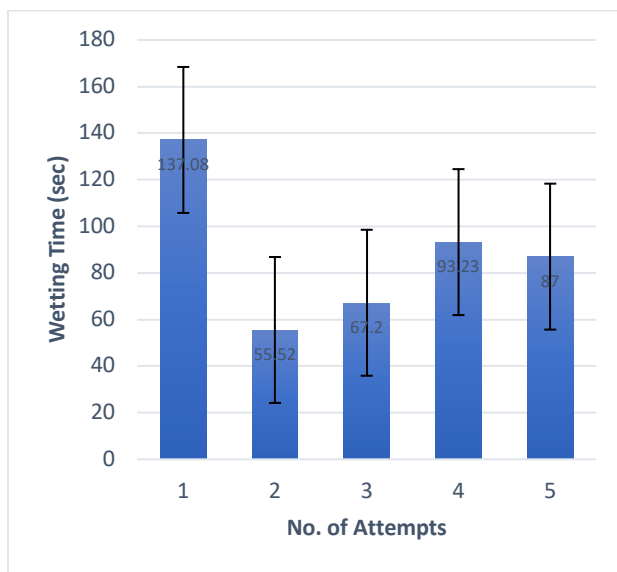


Figure E.1 Wetting Time (sec) Vs No. of Attempts of Uncoated Samples

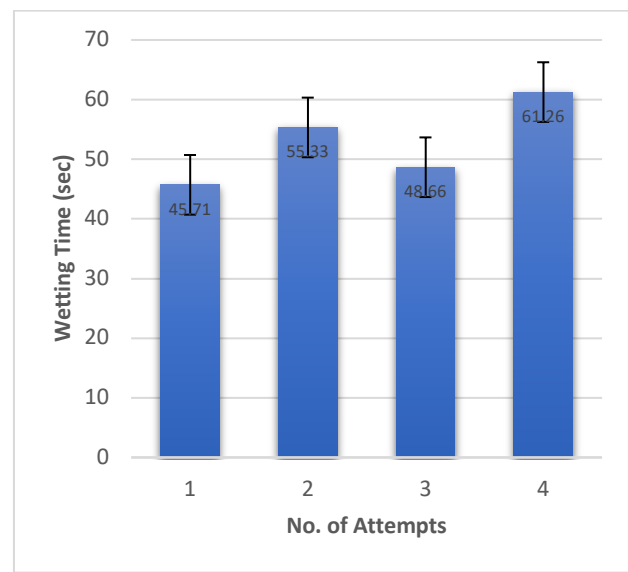


Figure E.2 Wetting Time (sec) Vs No. of Attempts of SiO₂ 1C Samples

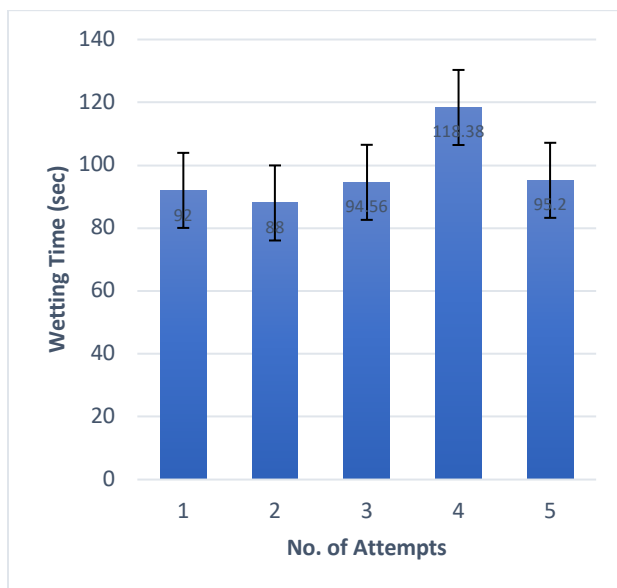


Figure E.3 Wetting Time (sec) Vs No. of Attempts of SiO₂ 2C Samples

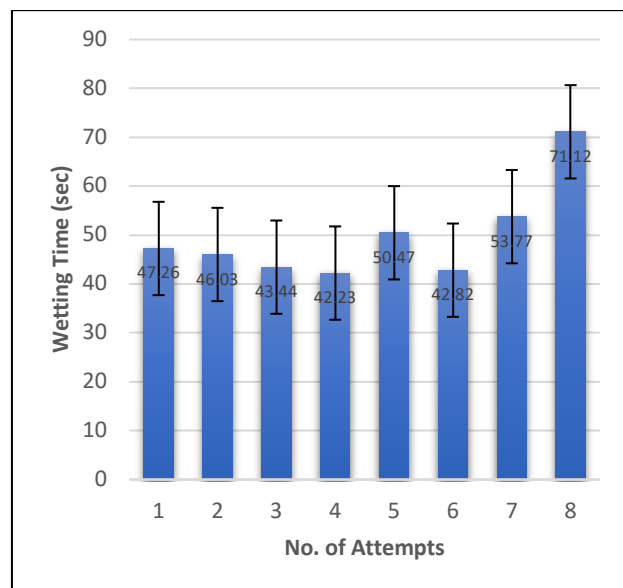


Figure E.4 Wetting Time (sec) Vs No. of Attempts of SiO₂ 3C Samples

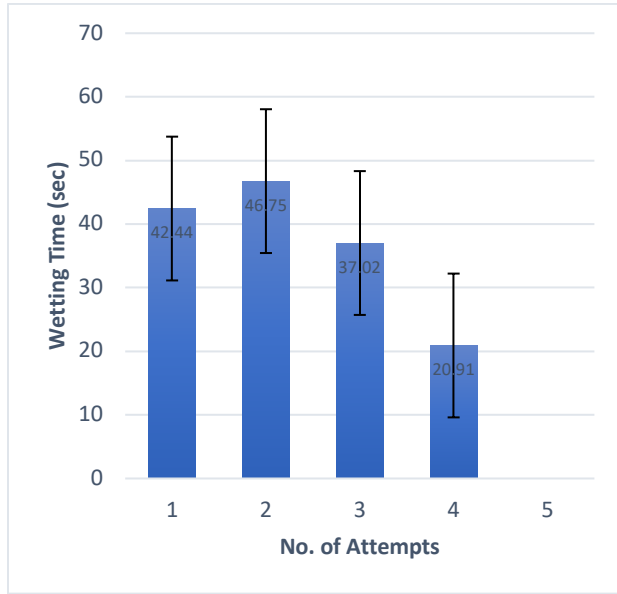


Figure E. 5 Wetting Time (sec) Vs No. of Attempts of SiO₂ 4C Samples

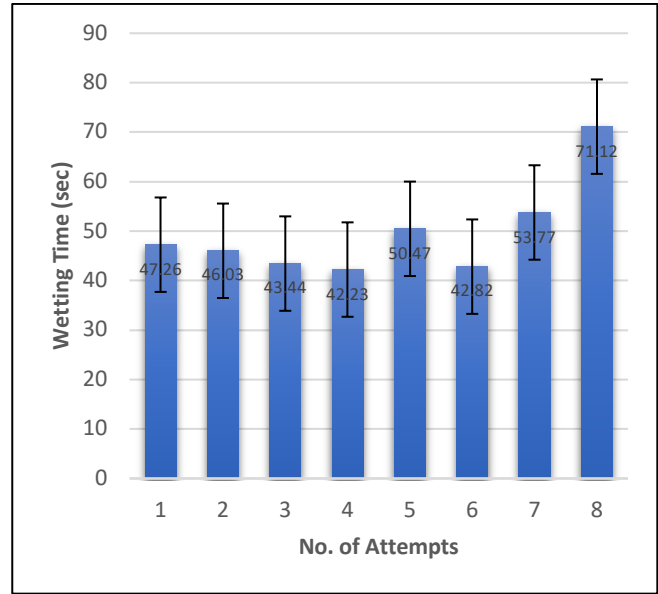


Figure E. 6 Wetting Time (sec) Vs No. of Attempts of SiO₂ 5C Samples

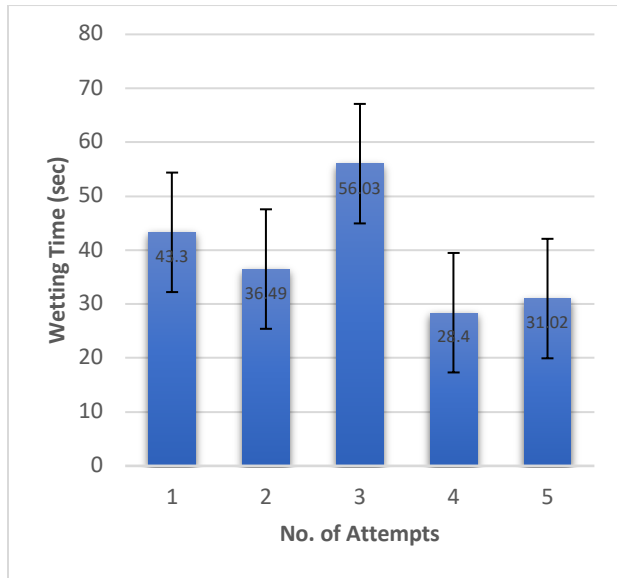


Figure E. 7 Wetting Time (sec) Vs No. of Attempts of SiO₂ 10C Samples

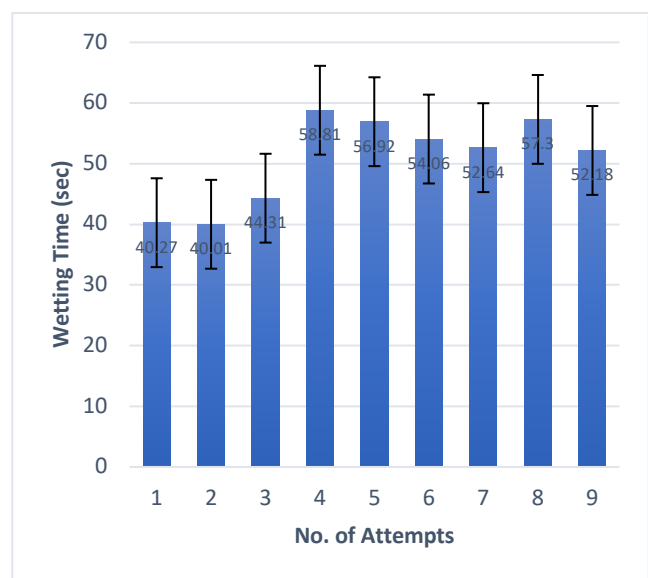


Figure E. 8 Wetting Time (sec) Vs No. of Attempts of TiO₂ 1C Samples

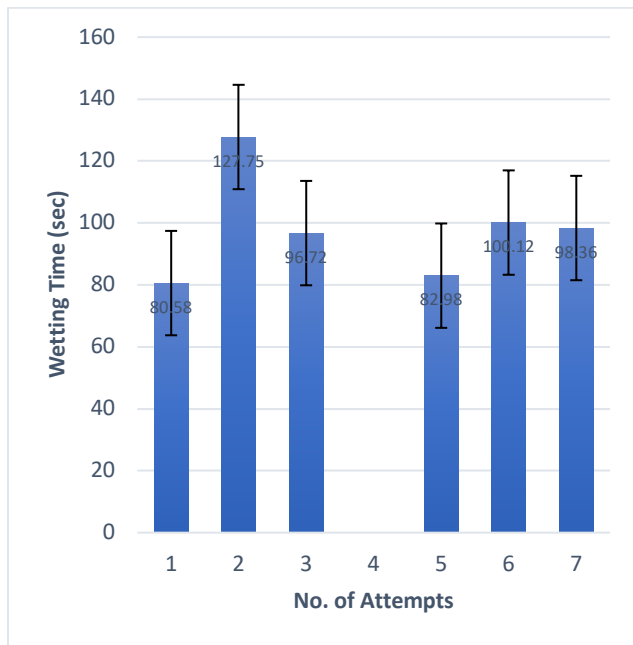


Figure E. 9 Wetting Time (sec) Vs No. of Attempts of TiO₂ 2C Samples

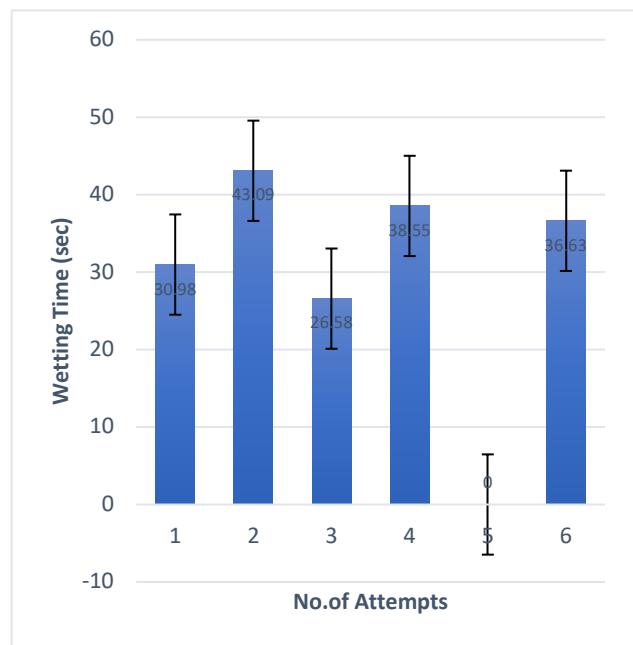


Figure E. 10 Wetting Time (sec) Vs No. of Attempts of TiO₂ 3C Samples

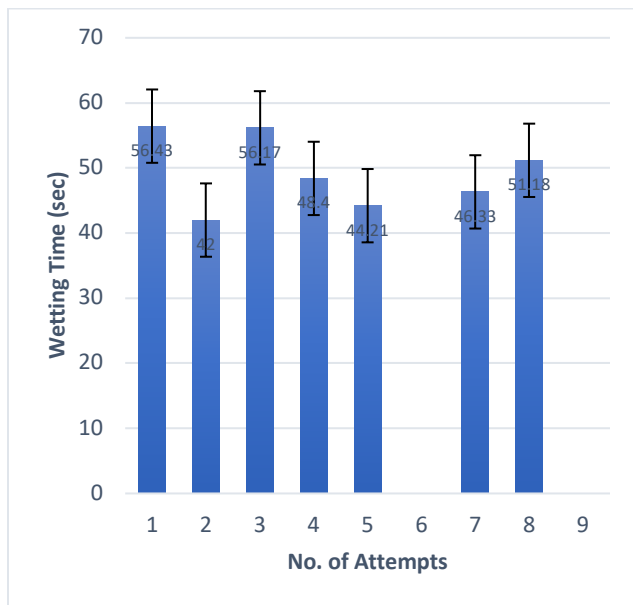


Figure E. 11 Wetting Time (sec) Vs No. of Attempts of TiO₂ 4C Samples

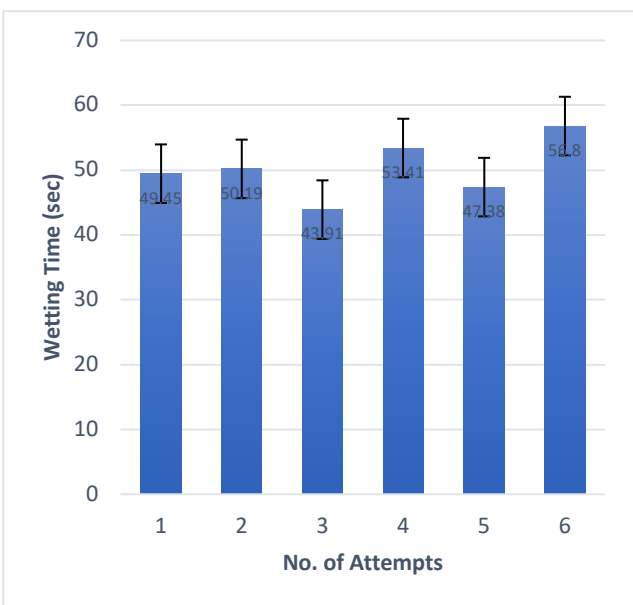


Figure E. 12 Wetting Time (sec) Vs No. of Attempts of TiO₂ 5C Samples

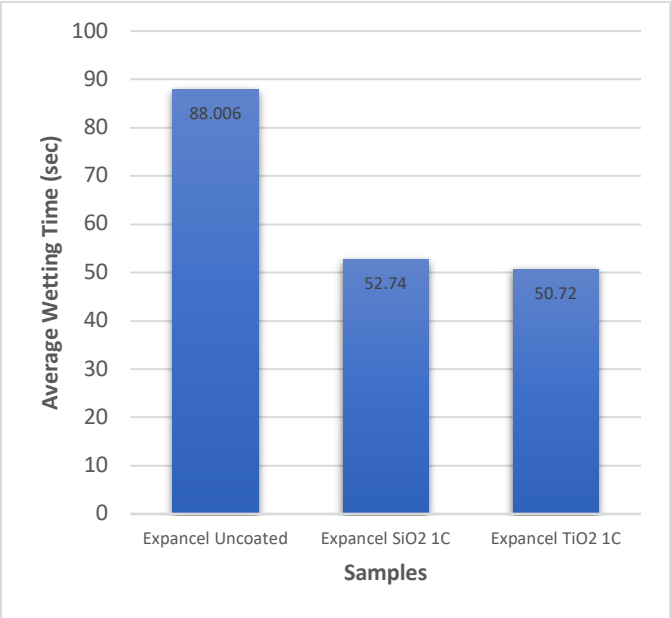


Figure E. 13 Average wetting time Vs Different samples